Density Functional Studies of a Heisenberg Spin Coupled Chromium−Semiquinone Complex and Its Chromium−Catechol Analog

Jorge H. Rodriguez,[1] Daniel E. Wheeler, and James K. McCusker*

Contribution from the Department of Chemistry, University of California at Berkeley, Berkeley, California 94720-1460

Received March 18, 1998. Revised Manuscript Received July 27, 1998

Abstract: The electronic structure of $[Cr(tren)(3,6\text{-DTBSQ})]^{2+}$, where tren is tris(2-aminoethyl)amine and 3,6-DTBSQ is 3,6-di-*tert*-butylorthosemiquinone, has been studied by self-consistent-field non-local gradient-corrected density functional theory. The results are consistent with a Heisenberg exchange formulation where a $Cr(S = {}^3/_2)$ ion is antiferromagnetically coupled to the semiquinone$(S = {}^1/_2)$ giving rise to a $S = 1$ ground state. Population analyses were carried out which show net α and β spin densities at the chromium ion and semiquinone, respectively. Some orbital interactions have been identified that allow partial delocalization from the semiquinone toward the chromium ion giving rise to an antiparallel alignment of their electron spins. The isotropic exchange constant J of the Heisenberg Hamiltonian $H_{ex} = J\mathbf{S}_1\cdot\mathbf{S}_2$ has been determined from the self-consistent-field energies at the U-BLYP/6-311** and U-B3LYP/6-311** levels and is consistent with previously reported magnetic susceptibility data. The triplet state wave function shows some spin contamination from the higher-lying quintet state. Accordingly, approximate spin and energy projections were performed to account for the quintet admixture. Some magneto-structural correlations between the $Cr-O_{SQ}$ and $O_{SQ}-C_{SQ}$ bond lengths and the magnitude of J have also been investigated. It was found that J decays in a nearly exponential fashion with increasing bond distances. The electronic structure of the free semiquinone ligand has also been studied and correlated to its bonding with chromium. Finally, a single-crystal X-ray structure of the related complex $[Cr(tren)(3,6\text{-DTBCat})]^+$ was obtained and used to carry out similar self-consistent-field calculations. Analysis of the quartet ground state wave function of the catecholate complex produced spin densities consistent with a $Cr(S = {}^3/_2)$−catechol$(S = 0)$ formulation.

I. Introduction

The chemistry and physical properties of complexes containing "non-innocent" ligands has attracted considerable interest. The most widely encountered class of these molecules are the quinoids whose "non-innocent" nature rests largely in their reversible redox chemistry:

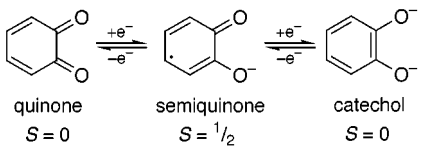

While the quinone form does not readily bind to transition metals, a large number of semiquinone and catecholate complexes of first-, second-, and some third-row metals are known. Over the last two decades, the study of transition metal−quinone compounds has developed into a rich field in terms of both synthetic and physical chemistries.[2−4] From the perspective of electronic structure theory, transition metal−semiquinone complexes are the most interesting owing to the radical nature of the semiquinone ligand. For example, the bonding between first-row transition metal cations, such as Cr^{3+} and Co^{2+}, and semiquinones produces compounds with unusual magnetic and optical properties[5−7] that appear to be governed by interactions between their unpaired electrons and the corresponding spin localized on the cation and radical. In contrast, the bonding between metallic cations and diamagnetic catechols produces complexes whose magnetism is characterized by the spin density of the metal alone.[5−7]

We have recently reported[7] on the synthesis, magnetic susceptibility, and optical properties of $[Cr(tren)(3,6\text{-DTBSQ})](PF_6)_2$, where tren is tris(2-aminoethyl)amine and 3,6-DTBSQ is 3,6-di-*tert*-butylorthosemiquinone. Magnetic susceptibility measurements on this complex revealed a temperature-independent effective magnetic moment of $2.85 \pm 0.10\ \mu_B$ in a 5−350 K range,[7] indicating a $S = 1$ ground state. In contrast, the catecholate analog with formula $[Cr(tren)(3,6\text{-DTBCat})](PF_6)$ exhibited a moment of $3.85 \pm 0.10\ \mu_B$[7] over the same temperature range, consistent with a $S = {}^3/_2$ ground state. The $S = 1$ ground state of the semiquinone complex was reasonably interpreted as arising from antiferromagnetic spin coupling between chromium and the semiquinone.[7] Indeed, this was also the explanation offered by Benelli *et al.*[5] in their original report on the chromium−semiquinone motif. These authors also

(1) Also at Department of Physics, University of Illinois at Urbana−Champaign, Urbana, IL 61801.

(2) Pierpont, C. G.; Buchanan, R. M. *Coord. Chem. Rev.* **1981**, *38*, 45.

(3) Pierpont, C. G.; Larsen, S. K.; Boone, S. R. *Pure Appl. Chem.* **1988**, *60*, 1331.

(4) Pierpont, C. G.; Lange, C. W. *Pure Appl. Chem.* **1994**, *41*, 331.

(5) Benelli, C.; Dei, A.; Gatteschi, D.; Güdel, H. U.; Pardi, L. *Inorg. Chem.* **1989**, *28*, 3089.

(6) Adams, D. M.; Noodleman, L.; Hendrickson, D. N. *Inorg. Chem.* **1997**, *36*, 3966.

(7) Wheeler, D. E.; McCusker, J. K. *Inorg. Chem.* **1998**, *37*, 2296.

10.1021/ja980917m CCC: $15.00
Published on Web 11/10/1998

reported the compound to be EPR silent, consistent with an integer spin ground state. Both groups rationalized the lack of temperature dependence of the effective magnetic moment as an indication of a large Heisenberg exchange constant (i.e., $|J| > 700$ cm^{-1}, $H_{ex} = J\mathbf{S}_1\cdot\mathbf{S}_2$), which prevents thermal population of the $S = 2$ excited (ferromagnetic) state. Further calculations by Benelli et al.[5] based on the assumption of a Tanabe mechanism for excited-state exchange[8,9] yielded a value of $J \approx 800$ cm^{-1}. However, the lack of thermal population of the quintet state in the temperature range of the susceptibility experiments casts some doubt as to the validity of describing the spin structure of these systems in terms of a Heisenberg exchange formalism. Consequently, it is of interest to apply theoretical methods to study the bonding and electronic structure of metal−semiquinone complexes to determine the physical origin of their unusual magnetism as well as the relevance of the Heisenberg spin coupling model. In addition, the relative simplicity of the chromium−semiquinone/catechol dyad made it very attractive from the standpoint of photophysical studies.[5,7] It is important to understand the electronic structure of these compounds as an aid in the interpretation of photophysical data. From a broader perspective, these systems are of great interest for understanding the bonding and magnetic interactions between a paramagnetic metal ion and a directly ligated organic-based spin center.

In this work we apply self-consistent-field Kohn−Sham density functional theory[10] to elucidate the electronic structure of [Cr(tren)(3,6-DTBSQ)]$^{2+}$. In particular, we have examined the bonding between chromium and a single semiquinone ligand and have identified some orbital interactions that give rise to the $S = 1$ ground state. The geometry of [Cr(tren)(3,6-DTBSQ)]$^{2+}$ has been optimized and compared with its crystallographic structure previously obtained from X-ray diffraction.[7] The total energies of the spin triplet and quintet states have been determined from self-consistent-field calculations on the optimized geometry and related to the magnitude of the Heisenberg exchange constant J. In addition, we present some magnetostructural information that correlates variations in geometry (i.e., Cr−O_{SQ} and O_{SQ}−C_{SQ} bond lengths) with the strength of antiferromagnetic exchange. Finally, the crystallographic structure of the related complex [Cr(tren)(3,6-DTB-Cat)]$^{+}$ has been obtained and used to perform additional calculations to determine the main characteristics of the chromium−catecholate bond.

II. Theoretical Background

The Kohn−Sham[10,11] formulation of density functional theory (DFT) is becoming widely applied to chemical problems such as the calculation of molecular energies and equilibrium geometries.[12,13] DFT methods can account for electron correlation at a computational cost that is low in comparison to other more conventional methods[14,15] such as Moller−Plesset perturbation theory (MP2). In particular, the relatively recent development of non-local and gradient-corrected exchange-correlation functionals[16−20] has made DFT a preferred method for treating large transition metal-containing molecules where correlation effects are important.[14,15]

Restricted open shell calculations[21] are incapable of describing weakly coupled spin centers since these produce a combination of singly- and doubly-occupied molecular orbitals. By contrast, unrestricted calculations allow α and β electrons to occupy orbitals with different spatial localization and, therefore, can describe the spin localized on two different paramagnetic centers. To allow for spin polarization[11] we have applied a spin unrestricted (U) open-shell formalism.[21] Within this framework, the Kohn−Sham Hamiltonian operator[10,11] gives rise to the following eigenvalue problem

$$H^{\mathrm{UKS}}\Phi_i^{\mathrm{UKS}}(\mathbf{r}) = \epsilon_i\Phi_i^{\mathrm{UKS}}(\mathbf{r}) \qquad (1)$$

where H^{UKS} includes electronic kinetic, electron−nuclear attraction, electron−electron repulsion, and exchange-correlation energy operators. In eq 1, the unrestricted Kohn−Sham molecular orbitals $\Phi_i^{\mathrm{UKS}}(\mathbf{r})$ have eigenvalues ϵ_i and are a linear expansion of sets of N basis functions $\{\phi_\mu(\mathbf{r})\}$

$$\Phi_i(\mathbf{r}) = \sum_{\mu=1}^{N} C_{\mu i}\phi_\mu(\mathbf{r}) \qquad (2)$$

The expansion coefficients $C_{\mu i}$ in (2) are obtained from the variational minimization of the total energy which is represented by H^{UKS}. Therefore, the Kohn−Sham calculations proceed in a manner that is analogous to conventional self-consistent field Hartree−Fock theory, the main difference being the treatment of electron exchange and correlation. Hartree−Fock calculations include exact non-local exchange and no electron correlation whereas DFT includes an exchange-correlation functional of the density.[11]

Heisenberg Antiferromagnetic Exchange Interaction. The interaction between the unpaired electrons of Cr^{3+} and the single unpaired electron of the semiquinone (SQ^{-}) can be represented by the Heisenberg Hamiltonian[22−31]

$$H_{ex} = J\mathbf{S}_1\cdot\mathbf{S}_2 \qquad (3)$$

In eq 3, J is a scalar that quantifies the isotropic exchange

(8) Gondaira, K.; Tanabe, Y. *J. Phys. Soc. Jpn.* **1966**, *21*, 1527.
(9) McCarthy, P. J.; Güdel, H. U. *Coord. Chem. Rev.* **1988**, *88*, 69.
(10) Kohn, W.; Sham, L. J. *Phys. Rev.* **1965**, *140*, A1133.
(11) Parr, R. G.; Yang, W. *Density-Functional Theory of Atoms and Molecules*; Clarendon Press: Oxford, 1989.
(12) Ziegler, T. *Chem. Rev.* **1991**, *91*, 651.
(13) Pople, J. A.; Gill, P. M. W.; Johnson, B. G. *Chem. Phys. Lett.* **1992**, *199*, 557.
(14) Siegbahn, P. E. M. In *New Methods in Computational Quantum Mechanics*; Prigogine, I., Rice, S. A., Eds.; John Wiley & Sons: New York, 1996.
(15) Head-Gordon, M. *J. Phys. Chem.* **1996**, *100*, 13213.
(16) Becke, A. D. *Phys. Rev. A* **1988**, *38*, 3098.
(17) Becke, A. D. *J. Chem. Phys.* **1993**, *98*, 1372.
(18) Becke, A. D. *J. Chem. Phys.* **1993**, *98*, 5648.
(19) Vosko, S. H.; Wilk, L.; Nusair, M. *Can. J. Phys.* **1980**, *58*, 1200.
(20) Lee, C.; Yang, W.; Parr, R. G. *Phys. Rev. B* **1988**, *37*, 785.
(21) Hehre, W. J.; Radom, L.; Schleyer, P. v. R.; Pople, J. A. *Ab Initio Molecular Orbital Theory*; John Wiley & Sons: New York, 1986.
(22) Heisenberg, W. *Z. Phys.* **1928**, *49*, 619.
(23) Anderson, P. W. *Phys. Rev.* **1959**, *115*, 2.
(24) Anderson, P. W. In *Magnetism*; Rado, G. T., Suhl, H., Eds.; Academic Press: New York; 1963 Vol. 1.
(25) Sinn, E. *Coord. Chem. Rev.* **1970**, *5*, 313.
(26) Ginsberg, A. P. *Inorg. Chim. Acta Rev.* **1971**, *5*, 45.
(27) Griffith, J. S. *Struct. Bonding* **1972**, *10*, 87.
(28) Owen, J.; Harris, E. A. In *Electron Paramagnetic Resonance*; Geschwind, S., Ed.; Plenum Press: New York, 1972.
(29) Bencini, A.; Gatteschi, D. *EPR of Exchange Coupled Systems*; Springer Verlag: Berlin, 1990.
(30) Kahn, O. In *Magneto-Structural Correlations in Exchange Coupled Systems*; Willet, R. D., Gatteschi, D., Kahn, O., Eds.; Reidel Publishing Co.: Dordrecht, 1985.
(31) Kahn, O. *Molecular Magnetism*; VCH: New York, 1993.

interaction[32] whereas $\mathbf{S}_1$ and $\mathbf{S}_2$ are the spin operators of Cr^{3+} and SQ^{-} with eigenvalues $S_1 = {}^3/_2$ and $S_2 = {}^1/_2$, respectively. It follows that the total spin operator $\mathbf{S} = \mathbf{S}_1 + \mathbf{S}_2$ has the eigenvalues $S_{min} = 1$ and $S_{max} = 2$ corresponding to the triplet ($2S_{min} + 1 = 3$) and quintet ($2S_{max} + 1 = 5$) states, respectively. In general, the eigenstates of H_{ex} have energies given by

$$E^{ex}_{2S+1} = {}^1/_2 J\{S(S+1) - S_1(S_1+1) - S_2(S_2+1)\} \quad (4)$$

It follows from eq 4 that the exchange interaction removes the degeneracy of the triplet and quintet states, giving rise to an energy splitting of magnitude $|E^{ex}_5 - E^{ex}_3|$. For antiferromagnetic exchange, the triplet is the ground state and is characterized by an antiparallel spin alignment of the two paramagnetic centers.

To determine the value of the exchange constant J from SCF density functional calculations, the energies of the projected (pure) triplet and quintet unrestricted Kohn−Sham (PUKS) wave functions can be written in terms of the Heisenberg energies given by eq 4. The exchange constant derived from these energies is then given by

$$J = 2\frac{E^{PUKS}_{2S_{max}+1} - E^{PUKS}_{2S_{min}+1}}{S_{max}(S_{max}+1) - S_{min}(S_{min}+1)} \quad (5)$$

The value of J derived from eq 5 that parametrizes the antiferromagnetic exchange of $[Cr(tren)(3,6\text{-DTBSQ})]^{2+}$ is, therefore

$$J = {}^1/_2(E^{PUKS}_5 - E^{PUKS}_3) \quad (6)$$

Energy Corrections for Spin Contamination. The high spin (i.e., ferromagnetic) state is the only pure state that can be described by a single determinant wave function.[31,33,34] Spin unrestricted ferromagnetic wave functions are generally found to be (nearly) pure as exemplified by conventional ab initio (UHF and MP2)[35,36] and DFT[37,34] results of previous authors. In general, however, the unrestricted Kohn−Sham wave functions obtained from SCF calculations are eigenfunctions of $\mathbf{S}_z$ but are not eigenfunctions of the total spin operator $\mathbf{S}^2$. As a consequence, the triplet (i.e., antiferromagnetic) single determinant wave function can have some admixture of higher spin states. Such an admixture implies that the triplet wave function is spin contaminated, mostly from the higher quintet. The admixture of higher spin states will shift the total SCF energy calculated with the contaminated triplet wave function (E^{UKS}_3) with respect to the corresponding energy of the pure state (E^{PUKS}_3). To estimate the energy shift introduced by the quintet admixture we developed an approximate method similar to the projection technique used by Yamaguchi *et al.*[36] for organic diradicals. First, we assume that the UKS wave function for the triplet state is essentially a linear combination of the normalized projected triplet and quintet wave functions. Such an assumption is valid when the expectation value of the total spin operator after spin annihilation[38,39] of the quintet is $\langle S^2\rangle_A \approx 2$. Accordingly, we write

$$\Phi^{UKS}_3 \approx C_3\Phi^{PUKS}_3 + C_5\Phi^{PUKS}_5 \quad (7)$$

Second, we make use of the normalization condition that follows from (7)

$$C_3^2 + C_5^2 \approx 1 \quad (8)$$

Third, the energy and spin expectation values of the contaminated triplet state are expanded in terms of the corresponding quantities of the projected states

$$E^{UKS}_3 = \langle\Phi^{UKS}_3|H^{UKS}|\Phi^{UKS}_3\rangle \approx C_3^2E^{PUKS}_3 + C_5^2E^{PUKS}_5 \quad (9)$$

$$(S^{UKS}_3)^2 = \langle\Phi^{UKS}_3|S^2|\Phi^{UKS}_3\rangle \approx C_3^2S_3(S_3+1) + C_5^2S_5(S_5+1) \quad (10)$$

Finally, from eqs 8−10 we obtain the following expressions for the energy of the projected triplet state and for the expansion coefficients of (7)

$$E^{PUKS}_3 \approx \frac{E^{UKS}_3 - C_5^2E^{PUKS}_5}{C_3^2} \quad (11)$$

$$C_3^2 = \frac{(S^{UKS}_3)^2 - S_5(S_5+1)}{S_3(S_3+1) - S_5(S_5+1)} \quad (12)$$

$$C_5^2 = \frac{S_3(S_3+1) - (S^{UKS}_3)^2}{S_3(S_3+1) - S_5(S_5+1)} \quad (13)$$

When the unrestricted Kohn−Sham wave functions for the quintet state are nearly pure (i.e., $\langle S^2\rangle \approx S(S+1)$), one can substitute E^{UKS}_5 for E^{PUKS}_5 in eq 11.

Some comments are relevant regarding the application of approximate spin projection methods in density functional theory. First, Pople *et al.*[40] pointed out that a single determinant of Kohn−Sham orbitals should properly exhibit spin contamination. Second, Yamanaka *et al.*[37] reported that spin-unrestricted Kohn−Sham density functional methods followed by approximate spin projection produced reasonable singlet−triplet energy gaps and reasonable values for the exchange constant J of some organic dimers. Furthermore, Wittbrodt and Schlegel[41] have warned about the improper use of spin projection in density functional theory applied to the calculation of potential energy surfaces. In general, these authors observed an overstabilization of the projected states which becomes more noticeable as the bond lengths increase with respect to their equilibrium values. Similarly, Goldstein *et al.*[42] in their calculation of singlet potential energy surfaces reported that spin projection overcorrects and concluded that the spin contaminated and spin projected energies provide upper and lower bounds to the true

(32) The $H_{ex} = J\mathbf{S}_1\cdot\mathbf{S}_2$ representation of the Heisenberg Hamiltonian is not universal. All the results given in this work are expressed in terms of this representation (i.e., eq (3). Other notations include $H_{ex} = -J\mathbf{S}_1\cdot\mathbf{S}_2$ and $H_{ex} = -2J\mathbf{S}_1\cdot\mathbf{S}_2$. To convert to these latter two notations, simply multiply J by -1 or $-{}^1/_2$, respectively.

(33) Hay, P. J.; Thibeault, J. C.; Hoffmann, R. J. *J. Am. Chem. Soc.* **1975**, *97*, 4884.
(34) Noodleman, L. *J. Chem. Phys.* **1981**, *74*, 5737.
(35) Yamaguchi, K.; Fukui, H.; Fueno, T. *Chem. Lett.* **1986**, *149*, 625.
(36) Yamaguchi, K.; Jensen, F.; Dorigo, A.; Houk, K. *Chem. Phys. Lett.* **1988**, *149*, 537.
(37) Yamanaka, S.; Kawakami, T.; Nagao, H.; Yamaguchi, K. *Chem. Phys. Lett.* **1994**, *231*, 25.
(38) Schlegel, H. B. *J. Chem. Phys.* **1986**, *84*, 4530.
(39) Schlegel, H. B. *J. Phys. Chem.* **1988**, *92*, 3075.
(40) Pople, J. A.; Gill, P. M. W.; Handy, N. *Int. J. Quantum Chem.* **1995**, *56*, 303.
(41) Wittbrodt, J. M.; Schlegel, H. B. *J. Chem. Phys.* **1996**, *105*, 6574.
(42) Goldstein, E.; Beno, B.; Houk, K. *N. J. Am. Chem. Soc.* **1996**, *118*, 6036.

Table 1. Crystallographic Data for [Cr(tren)(3,6-DTBCat)](ClO_4)·THF·$^1/_2H_2O$·NaC1O_4

empirical formula[a]	$CrC_{26}N_4H_{50}Cl_{1.5}O_{10}Na_{0.5}$
formula wt	694.75
crystal color, habit	green, plate
crystal system	triclinic
space group	$P\bar{1}$ (No. 2)
temp (K)	178 ± 1
cell dimens:	
a (Å)	11.0689(7)
b (Å)	15.2390(10)
c (Å)	21.5543(14)
α (deg)	83.697(1)
β (deg)	84.186(1)
γ (deg)	70.623(1)
V (Å^3)	3400.9(3)
Z	4
goodness of fit (*S*)[b]	1.62
R[c]	0.059
R_w[d]	0.051

[a] The empirical formula is based on 1 equiv of the chromium complex. [b] $S = [\sum w(|F_o| - |F_c|)^2/(m-n)]^{1/2}$. [c] $R = ||F_o| - |F_c||/\sum|F_o|$. [d] $R_w = [\sum w(|F_o| - |F_c|)^2/\sum|F_o|^2]^{1/2}$.

energy. Therefore, the projected energies obtained from eq 11, particularly away from the equilibrium geometries, are not necessarily more accurate but, nevertheless, constitute useful estimates of their lower limit. Our present application of eq 11 is for triplet−quintet splittings at equilibrium geometries where approximate spin projection has given more accurate results.[37,41,42]

III. Materials and Methods

Synthesis and X-ray Crystallography of [Cr(tren)(3,6-DTBCat)](ClO_4). The synthesis of [Cr(tren)(3,6-DTBCat)](PF_6) has been previously described.[7] The perchlorate salt for which X-ray quality single crystals were obtained was prepared by dissolving [Cr(tren)(3,6-DTBCat)](PF_6) in ethyl acetate. An aqueous solution of $NaClO_4$ was added and the product was extracted into ethyl acetate (3 × 30 mL). Rotary evaporation afforded a green powder. A crystalline product was obtained by diffusing pentane into an ether/THF solution of the compound.

A single-crystal X-ray structure determination of [Cr(tren)(3,6-DTBCat)](ClO_4) was carried out at the CHEXRAY facility of the Department of Chemistry, University of California at Berkeley. Green plates of [Cr(tren)(3,6-DTBCat)](ClO_4) were obtained by diffusion of pentane into an ether/THF solution of the compound. One crystal having approximate dimensions of 0.28 × 0.24 × 0.10 mm was mounted on a glass fiber with Paratone N hydrocarbon oil. Diffraction data were collected on a Siemens SMART diffractometer using graphite monochromated Mo Kα radiation. Data were collected at −95 °C. Details regarding the structure determination are listed in Table 1, and positional parameters are listed in Table 2. The unit cell parameters were obtained by a least-squares refinement by using the measured positions of 5944 reflections with $I > 10\sigma$ in the range of $3.00° < 2\theta < 45°$. Intensity data were corrected for Lorentz and polarization effects; no decay correction was applied. An empirical absorption correction based on a comparison of redundant and equivalent reflections was applied by using the program SADABS[43] ($T_{max} = 0.86$, $T_{min} = 0.65$). The structure was solved by direct methods and expanded with Fourier techniques. All non-hydrogen atoms except for the ClO_4^- anions and the THF and water solvate molecules (vide infra) were refined anisotropically while the rest were refined isotropically. Hydrogen atoms were included at calculated positions[44] except those of the water solvate (H101 and H102). These latter hydrogens were placed in the positions of peaks found in the difference Fourier map but were not refined. The final cycle of least-squares refinement was based on 5273 observed reflections and 775 variables, resulting in unweighted and weighted *R* factors of 0.059 and 0.051, respectively.

Table 2. Atomic Positional Parameters and Equivalent Isotropic Thermal Parameters for Cation 1 of [Cr(tren)(3,6-DTBCat)](ClO_4)·THF·$^1/_2H_2O$·$^1/_2$NaClO_4

atom	*x*/*a*	*y*/*b*	*z*/*c*	B_{eq} (Å^2)
Cr(l)	−0.23267(10)	0.02178(7)	0.20606(5)	2.15(3)
O(1)	−0.3754(4)	−0.0199(3)	0.23390(18)	1.84(11)
O(2)	−0.1941(4)	−0.0018(3)	0.2919(2)	2.46(12)
N(1)	−0.0788(5)	0.0690(4)	0.1706(3)	2.55(15)
N(2)	−0.0877(5)	−0.1079(4)	0.1968(2)	2.73(15)
N(3)	−0.3192(5)	0.1613(4)	0.2221(3)	3.06(15)
N(4)	−0.2717(5)	0.0407(4)	0.1110(3)	2.72(15)
C(1)	−0.6160(6)	−0.0435(5)	0.2986(3)	2.43(18)
C(2)	−0.1877(7)	−0.0596(7)	0.1989(4)	5.7(3)
C(3)	−0.1696(7)	−0.0374(5)	0.4283(3)	3.1(2)
C(4)	−0.7256(7)	−0.0526(6)	0.3455(3)	4.3(2)
C(5)	−0.5895(6)	−0.1192(5)	0.2539(3)	3.1(2)
C(6)	−0.6639(6)	0.0524(5)	0.2626(4)	3.6(2)
C(7)	−0.0459(6)	−0.1093(5)	0.4049(3)	3.6(2)
C(8)	−0.1586(8)	0.0596(6)	0.4169(4)	5.6(3)
C(9)	0.0316(7)	0.0024(6)	0.2018(3)	3.7(2)
C(10)	0.0412(7)	−0.0964(6)	0.1932(4)	3.9(2)
C(11)	−0.1069(8)	0.1671(6)	0.1867(4)	4.2(2)
C(12)	−0.0635(7)	0.0638(5)	0.1014(3)	3.4(2)
C(13)	−0.2147(8)	0.1924(5)	0.2371(4)	4.3(2)
C(14)	−0.1925(7)	0.0944(5)	0.0748(3)	3.4(2)
C(15)	−0.3886(6)	−0.0330(4)	0.2982(3)	1.64(16)
C(16)	−0.2874(6)	−0.0266(4)	0.3293(3)	1.94(17)
C(17)	−0.2820(6)	−0.0429(4)	0.3943(3)	2.26(17)
C(18)	−0.3871(7)	−0.0657(5)	0.4261(3)	2.9(2)
C(19)	−0.4883(6)	−0.0677(5)	0.3955(3)	2.8(2)
C(20)	−0.4963(6)	−0.0498(4)	0.3308(3)	1.98(17)

Two independent chromium cations were found in the asymmetric unit. These cations are virtually identical in their metric details save for slight differences in the torsional angles of the methylene linkages of the tren ligand and somewhat larger thermal ellipsoids for some of the carbon atoms of the tren. In addition to the THF and H_2O solvate molecules alluded to above, 1 equivalent of $NaClO_4$ was found to have co-crystallized with the complex. Each sodium ion is hexacoordinate and exists as a dimeric complex in the lattice with both terminal (2) and bridging (2) perchlorate ions in the coordination sphere. The sodium ion of the asymmetric unit lies near the inversion center, making the dimer symmetric about the midpoint of the $Na_2(\eta-ClO_4)_2$ unit. The remaining four sites on each sodium ion are occupied by the water and THF solvates and the two η_1-ClO_4 ions.

Computational Procedures. Two main combinations of exchange and correlation density functionals were used for the self-consistent field (SCF) calculations. First, we applied the three-parameter exchange of Becke[16−19] in conjunction with the Lee−Yang−Parr[20] correlation functional (B3LYP). Such a combination constitutes a hybrid method that combines Hartree−Fock[21,45−47] with Slater[10,48,49] and gradient-corrected Becke[16−18] exchange functionals. Within the B3LYP method, the correlation is introduced by a combination of the local and nonlocal functionals of Vosko−Wilk−Nusair[19] and Lee−Yang−Parr,[20] respectively. Second, we used a combination of the Becke[16] gradient-corrected exchange and nonlocal Lee−Yang−Parr[20] correlation functionals (BLYP).

Two types of basis sets were used during the course of the SCF calculations, namely 6-311G** and LanL2DZ. The structure obtained from X-ray crystallography was used to perform the geometry optimization of $[Cr(tren)(3,6\text{-}DTBSQ)]^{2+}$ at the U-B3LYP/LanL2DZ

(43) SADABS, Siemens Area Detector Absorption Correction Program, G. Sheldrick Siemens Energy & Automation, Inc., Madison, WI, 1996.
(44) teXsan, Crystal Structure Analysis Package, Molecular Structure Corporation, 1992.
(45) Hartree, D. R. *Proc. Cambridge Philos. Soc.* **1927**, *24*, 89.
(46) Fock, V. *Physik* **1930**, *61*, 126.
(47) Hartree, D. R. *The Calculation of Atomic Structure*; Wiley: New York, 1957.
(48) Hohenberg, P.; Kohn, W. *Phys. Rev.* **1964**, *136*, B864.
(49) Slater, J. C. *Quantum Theory of Molecules and Solids. Vol. 4: The Self-Consistent Field for Molecules and Solids*; McGraw-Hill: New York, 1974.

level. The LanL2DZ[50−53] basis set includes the Dunning−Huzinaga[50] double-ζ functions for first-row elements and Los Alamos effective core potentials plus double-ζ functions[51−53] for chromium. Effective core potentials were used to account for the ten core electrons of chromium, but all other electrons in the molecule were included during the geometry optimization. The resulting optimized geometry was used to perform further single-point self-consistent field, nonlocal, gradient-corrected density functional calculations.

The single-point calculations, designed to obtain accurate total and molecular orbital energies for free semiquinone, [Cr(tren)(3,6-DTBSQ)]$^{2+}$, and [Cr(tren)(3,6-DTBCat)]$^{+}$ were done with the all-electron 6-311G** basis set.[21] The calculations for [Cr(tren)(3,6-DTBCat)]$^{+}$ were done with the experimental geometry. All atoms were included in the single-point SCF calculations at the U-BLYP/6-311G** and U-B3LYP/6-311G** levels. For [Cr(tren)(3,6-DTBSQ)]$^{2+}$ these included a total of 742 basis functions and 1183 primitive gaussians. Separate calculations were performed to determine the energies and Kohn−Sham wave functions corresponding to the triplet and quintet states of [Cr(tren)(3,6-DTBSQ)]$^{2+}$.

The Gaussian-94[54] electronic structure package was used to carry out all SCF single-point calculations and geometry optimizations. The SCF energies of [Cr(tren)(3,6-DTBSQ)]$^{2+}$ were obtained by using a tight[55] convergence criterion. The wave functions were analyzed with MOLDEN[56] to plot electronic density contours. Analyses of atomic charge, spin densities, and atomic orbital occupancies were performed within the natural population analysis (NPA) framework developed by Weinhold *et al.*[57−60] Within this framework, the atom-centered basis set $\{\phi_\mu(\mathbf{r})\}$ used to expand the unrestricted Kohn−Sham orbitals (eq 2) has been transformed into a complete orthonormal set of natural localized atomic orbitals (NAO).[57−59] In addition, the standard Mulliken population analyses have been performed. Computations were carried out on the IBM-SP2 and IBM-J40 parallel processing computers of the University of Illinois Research Computing Cluster (RCC), the HP-Convex SPP-2000 system of the National Center for Supercomputer Applications (NCSA), and the IBM-SP2 cluster of Mahui High Performance Computing Center (MHPCC).

IV. Results and Discussion

A. Crystallographic Structure of [Cr(tren)(3,6-DTBCat)](ClO$_4$). To compare the electronic structures of the chromium−semiquinone and chromium−catechol complexes, a single-crystal X-ray structure of the catecholate complex was needed. Numerous attempts to grow crystals of the PF_6 salt in the course of our previous study[7] were unsuccessful. However, following metathesis to the ClO_4 salt, we were able to obtain X-ray quality crystals by diffusion of pentane into a THF/ether solution of the compound. [Cr(tren)(3,6-DTBCat)](ClO_4) crystallizes in the tricinic space group $\bar{1}$ with two independent chromium cations in the asymmetric unit. In addition, THF and H_2O molecules as well as 1 equiv of $NaClO_4$ have been found to co-crystallize with the complex. Crystallographic details are given in Table 1. The two cations in the structure are essentially identical except for minor differences in certain metric details (Section III). Thus, for simplicity, we shall restrict our discussion of the structure to cation 1 (i.e., Cr1), which was used to perform the self-consistent field calculations reported in this work. Positional parameters and selected bond distances and angles for cation 1 are given in Tables 2 and 3, respectively; an ORTEP drawing of this cation is shown in Figure 1. The chromium center is six-coordinate with four aliphatic nitrogens from the tren ligand and two oxygen donors from the bound catechol. Bond angles about the metal center deviate somewhat from 90° and 180° due largely to the restricted bite angle of the tren ligand, resulting in a distorted octahedral coordination environment. The Cr−N bond distances are unremarkable with an average value of 2.098 Å, slightly longer than the corresponding average for the semiquinone analog (2.07 Å).[7] A difference between the catecholate and semiquinonate X-ray structures is also noted in the Cr−O bond distances. In the first compound, these two bonds are essentially identical (i.e., 1.910(4) and 1.911(4) Å for Cr1−O1 and Cr1−O2, respectively), whereas a larger difference was noted in the semiquinone complex[7] (Table 3). This likely reflects the difference in oxidation state of the ligands in these compounds and serves as a secondary indicator of the nature of the quinoidal ligand in the complex.

The strongest structural evidence of the oxidation state of the quinoid ligand is generally taken from the C−C and C−O bond distances. The nonaromatic nature of the semiquinone

Table 3. Selected Bond Lengths (Å) and Angles (deg) for Cation 1 of [Cr(tren)(3,6-DTBCat)](ClO_4)·THF·$^1/_2H_2O$·$^1/_2NaClO_4$ and [Cr(tren)(3,6-DTBSQ)]$^{2+}$

	[Cr(tren)(3,6-DTBCat)]$^{+}$	[Cr(tren)(3,6-DTBSQ)]$^{2+}$	
	expt[a]	expt[b]	U-B3LYP[c]
	bond lengths		
Cr(1)−O(1)	1.910(4)	1.937(4)	1.944
Cr(1)−O(2)	1.911(4)	1.901(4)	1.918
Cr(1)−N(1)	2.105(5)	2.055(6)	2.106
Cr(1)−N(2)	2.074(5)	2.089(5)	2.132
Cr(1)−N(3)	2.107(5)	2.072(5)	2.123
Cr(1)−N(4)	2.106(5)	2.064(5)	2.113
O(1)−C(1)	1.372(7)	1.312(8)	1.353
O(2)−C(2)	1.378(7)	1.293(7)	1.346
C(1)−C(2)	1.397(8)	1.442(10)	1.479
C(1)−C(6)	1.401(8)	1.429(9)	1.425
C(2)−C(3)	1.405(8)	1.445(9)	1.431
C(3)−C(4)	1.398(9)	1.353(10)	1.396
C(4)−C(5)	1.366(9)	1.43(1)	1.440
C(5)−C(6)	1.413(8)	1.36(1)	1.400
	bond angles		
O(1)−Cr(1)−O(2)	84.67(2)	81.6(2)	81.2
O(1)−Cr(1)−N(1)	98.3(2)	99.2(2)	99.5
O(1)−Cr(1)−N(2)	88.0(2)	87.2(2)	86.1
O(1)−Cr(1)−N(3)	83.5(2)	88.0(2)	86.5
O(1)−Cr(1)−N(4)	177.2(2)	175.9(2)	176.5
O(2)−Cr(1)−N(1)	177.0(2)	177.9(2)	179.2
O(2)−Cr(1)−N(2)	97.9(2)	99.1(2)	96.6
O(2)−Cr(1)−N(3)	99.9(2)	95.1(2)	96.7
O(2)−Cr(1)−N(4)	94.6(2)	95.3(2)	95.3
Cr(1)−O(1)−C(1)	112.1(2)	114.3(2)	116.2
Cr(1)−O(2)−C(2)	111.6(2)	115.5(2)	117.5

[a] Obtained from single-crystal X-ray diffraction. [b] Obtained from single-crystal X-ray diffraction by Wheeler *et al.*[7] [c] Parameters from a geometry optimization at the U-B3LYP/LanL2DZ level.

(50) Dunning, T. H.; Hay, P. J. In *Modern Theoretical Chemistry*; Schaefer, H. F. I., Ed.; Plenum: New York, 1976.
(51) Hay, P. J.; Wadt, W. R., *J. Chem. Phys.* **1985**, *82*, 270.
(52) Wadt, W. R.; Hay, P. J. *J. Chem. Phys.* **1985**, *82*, 284.
(53) Hay, P. J.; Wadt, W. R. *J. Chem. Phys.* **1985**, *82*, 299.
(54) Gaussian 94, Revision E.2, M. J. Frisch, G. W. Trucks, H. B. Schlegel, P. M. W. Gill, B. G. Johnson, M. A. Robb, J. R. Cheeseman, T. Keith, G. A. Petersson, J. A. Montgomery, K. Raghavachari, M. A. Al-Laham, V. G. Zakrzewski, J. V. Ortiz, J. B. Foresman, J. Cioslowski, B. B. Stefanov, A. Nanayakkara, M. Challacombe, C. Y. Peng, P. Y. Ayala, W. Chen, M. W. Wong, J. L. Andres, E. S. Replogle, R. Gomperts, R. L. Martin, D. J. Fox, J. S. Binkley, D. J. Defrees, J. Baker, J. P. Stewart, M. Head-Gordon, C. Gonzalez, and J. A. Pople; Gaussian, Inc.: Pittsburgh, PA, 1995.
(55) Frisch, M. J.; Frisch, A.; Foresman, J. B. *Gaussian 94 User's Manual*; Gaussian Inc.: Pittsburgh, 1995.
(56) MOLDEN, Molecular Density Package, G. Schaftenaar, CAOS/CAMM Center Nijmegen, The Netherlands, 1991.
(57) Reed, A. E.; Weinhold, F. *J. Chem. Phys.* **1983**, *78*, 4066.
(58) Reed, A. E.; Weinstock, R. B.; Weinhold, *F. J. Chem. Phys.* **1985**, *83*, 735.
(59) NBO 3.1, E. D. Glendening, A. E. Reed, J. E. Carpenter, and F. Weinhold, Theoretical Chemistry Institute, University of Wisconsin, Madison, 1996.
(60) NBO 4.0, E. D. Glendening, J. K. Badenhoop, A. E. Reed, J. E. Carpenter, and F. Weinhold, Theoretical Chemistry Institute, University of Wisconsin, Madison, 1996.

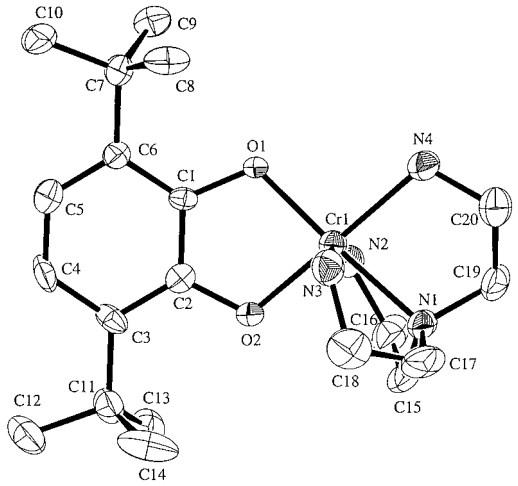

Figure 1. Drawing of the cation of [Cr(tren)(3,6-DTBCat)]ClO_4 obtained from a single-crystal X-ray structure determination. See Tables 1−3 for the corresponding crystallographic data. This perspective is roughly looking down the *z* axis defined by Figure 2.

ligand in $[Cr(tren)(3,6\text{-}DTBSQ)]^{2+}$ was clearly seen from the alternating single/double bond character of some C−C bonds. Upon one-electron reduction to form the catecholate, an aromatic species is expected with six nearly identical C−C bond distances. This is true for free catechol, where all of the ring bond distances are found to be identical to within 0.005 Å at 1.385 Å.[61,62] However, when bound to a metal center this equivalency of the C−C bonds is, to some extent, lost despite the fact that the catechol nature of the ligand can be verified by other means. For example, Raymond and co-workers[63] reported the X-ray crystal structure of $[Cr(3,5\text{-}DTBCat)_3]^{3-}$ for which magnetic data unambiguously indicated a formulation of Cr^{3+} and three diamagnetic catechols. While variations in C−C bond distances within the catecholate complex are not nearly as pronounced as in the semiquinone analog, they do cover a surprisingly large range. The average bond distance is 1.397 Å and the individual values range from 1.366(9) Å for C4−C5 to 1.413(8) Å for C5−C6. Again, when compared to the structure of $[Cr(tren)(3,6\text{-}DTBSQ)]^{2+}$, it is clear that the bond distances in the catecholate complex span a much narrower range and are not describable in terms of the (overall) alternating character used for the semiquinone. It is nonetheless curious that coordination to the chromium center does appear to significantly alter the aromaticity of the catecholate relative to its disposition as a free ligand.

The C−O bond distances can also be used as indicators of the quinone oxidation state. In the semiquinone complex, these two bond distances were somewhat different, consistent with the pseudo-double-bond and single-bond character of the C−O fragments (Table 3). The difference between these bonds is statistically negligible in the catecholate complex with C1−O1 and C2−O2 distances of 1.372(7) and 1.378(7) Å, respectively. These lengths agree well with the value of ca. 1.35 Å that has been reported for other first-row metal−catecholate complexes,[2] confirming that a catechol formulation for the ligand is appropriate in the present case.

B. Geometry Optimization of $[Cr(tren)(3,6\text{-}DTBSQ)]^{2+}$. While, at present, performing optimizations of transition metal-containing molecules of some 20−30 atoms is considered computationally practical,[14] the optimization of larger systems is less common due to the computational expense involved. Nevertheless, we have performed a geometry optimization for the triplet state of $[Cr(tren)(3,6\text{-}DTBSQ)]^{2+}$ including all 65 atoms. The X-ray structure[7] was used as the starting input. By using a U-B3LYP/LanL2DZ model chemistry, convergence with Gaussian-94[54] was achieved. The Cartesian coordinates of the optimized geometry are given in Supplementary Table 5. The total energy of the equilibrium (optimized) geometry was ≈0.539 hartrees (≈14.7 eV) lower than the corresponding energy of the X-ray structure.

Table 3 shows some bond lengths and angles for the X-ray[7] and optimized geometries of the semiquinone complex. The main trends observed in the X-ray structure are also reproduced by the optimized geometry. For example, the optimized structure predicted a 0.026 Å difference between the Cr1−O1 and Cr1−O2 bond lengths. While the optimized geometry is consistent with the X-ray structure, which yielded a 0.036 Å difference between Cr1−O1 and Cr1−O2, it also increased these lengths by 0.007 and 0.017 Å, respectively. Based on their optimized bond lengths we found two main types of C−C bonds in the ring of complexed semiquinone: C1−C2 (1.479 Å) and C4−C5 (1.440 Å) have lengths close to those expected for a single bond, whereas C3−C4 and C5−C6 have nearly equal lengths close to those expected for a weak double bond (≈1.400 Å).

The spatial parameters of the hydrogens were added to the original X-ray structure at positions calculated with teXsan.[44] Typically, the hydrogen positions determined from X-ray crystallography programs correspond to a minimization of residual densities and do not correspond to proton positions.[64] Therefore, it is of interest to determine optimized parameters corresponding to proton positions that minimize the total energy. For example, the optimized bond lengths for H−C4 and H−C5 were 1.084 Å whereas the teXsan[44] distances, corresponding to residual peaks, were 0.946 and 0.983 Å, respectively. The teXsan H−C4−C5 and H−C5−C4 angles were 118.32° and 116.43°, respectively, whereas the corresponding optimized values were 116.77° and 116.86°. Similar trends were found for the other hydrogen atom bonding lengths and angles of the molecule. Thus, while teXsan[44] produced angles which are within 1% of those predicted by DFT, the corresponding distances were ≈12−15% shorter than the proton positions determined from DFT.

The geometry of free semiquinone was also optimized. It shows a clear trend of alternating shorter and longer distances between the carbons of the six-membered ring which is only altered by a longer character of C1−C2 (1.518 Å). The equilibrium lengths predicted for the C−C bonds of the ring in free semiquinone are very close to the corresponding lengths of the complexed ligand with the exception of C1−C2 which is longer in the first case.

C. Electronic Structure of the Semiquinone Radical. To understand the magnetic interaction between chromium and the semiquinone ligand, we performed SCF density functional calculations on free semiquinone at the U-BLYP/6-311G** and U-B3LYP/6-311G** levels. The two exchange-correlation functionals produced slightly different MO energy schemes. The relative order of MOs 58 and 59 is reversed for the U-BLYP and U-B3LYP functionals whereas the order of MOs 60, 61, and 62 is the same. The SCF calculations in both cases yielded

(61) Brown, C. J. *Acta. Crystallogr.* **1966**, *21*, 170.
(62) Wanderlich, H.; Mootz, D. *Acta Crystallogr. B* **1971**, *27*, 1684.
(63) Sofen, S. R.; Ware, D. C.; Cooper, S. R.; Raymond, K. N. *Inorg. Chem.* **1979**, *18*, 234.

(64) As pointed out by one of the reviewers of this manuscript.

Table 4. Energies, Main Composition, and Semiquinone−Metal Bonding Character of Frontier Molecular Orbitals of Semiquinone Radical Obtained at the U-BLYP/6-311G** Level

orbital	type[a]	energy (eV)	U-BLYP composition[b]	SQ−Cr bond[c]
62α	V	+3.407	C3,C6(p_z)	π
61α	O	+0.249	O1,O2(p_z)	π
60α	O	−0.517	O1,O2(p_y)	π
59α	O	−1.070	O1,O2(p_y)	σ
58α	O	−1.277	C3,C6(p_z)	π
61β	V	+0.769	O1,O2(p_z)	π
60β	O	−0.375	O1,O2(p_y)	π
59β	O	−0.917	O1,O2(p_y)	σ
58β	O	−0.982	C3,C6(p_z)	π

[a] V and O represent virtual (unoccupied) and occupied molecular orbitals, respectively. [b] The composition indicates the specific atoms and corresponding orbitals where the free semiquinone MOs are mainly localized. [c] The SQ−Cr bonding character indicates the type of bonding allowed between semiquinone MOs and Cr orbitals.

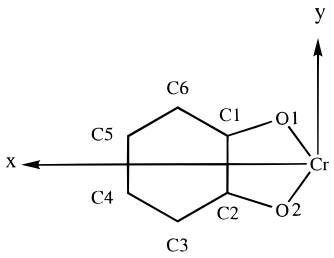

Figure 2. Coordinate system used as reference for the description of molecular orbitals (MOs) and natural atomic orbitals (NAOs). The *z* axis (not shown) is pointing out of the *xy* plane forming a right-handed coordinate system.

essentially pure doublet ground state wave functions with spin expectation values $\langle S^2 \rangle \approx 0.75$.

Table 4 lists the U-BLYP energies, main composition, and ligand−metal bonding character of the frontier semiquinone molecular orbitals. Our results are in qualitative agreement with those reported by Adams *et al.*[6] The coordinate system used for the calculations is shown in Figure 2. The semiquinone ring and oxygen atoms lie on the *xy* plane. In what follows we describe some characteristics of the individual U-BLYP molecular orbitals. The two-dimensional contour plots of the electron density discussed below (Figures 3−7) are slices taken 0.5 Å above the O−Cr−O plane for MOs 58, 61, and 62 and at the O−Cr−O plane for MOs 59 and 60.

Occupied MOs 58α and 58β are mostly composed of p_z orbitals localized on C3 and C6 and a lesser contribution from C4 and C5. In addition, there is a contribution from oxygen p_z orbitals that combine in a π-antibonding fashion with the carbon orbitals. The contour of Figure 3 shows the antibonding interaction between oxygen and carbon atoms. The electron density is localized above and below the plane of the ring. Due to their composition MOs 58 can combine in a π fashion with metal orbitals of d_{yz} symmetry.

Occupied MOs 59α and 59β are mostly a combination of oxygen p_y and p_x orbitals. As a result, these MOs lie in the *xy* plane with dominant p_y character. As shown in the contour of Figure 4, there is a weak σ-antibonding interaction between the orbitals of the two oxygens. Due to their composition, MOs 59 can combine in a σ fashion with metal orbitals of d_{xy} symmetry.

MOs 60α and 60β have main contributions from O(p_y) orbitals (Figure 5). In addition, there is some electron density localized on p_y orbitals of C1 and C2. As shown in the two-dimensional contour of Figure 5, there is an antisymmetric combination of oxygen and carbon orbitals that results in a weak side-on interaction. Due to their composition, MOs 60 can combine in a π fashion with metal orbitals of $d_{x^2-y^2}$ symmetry.

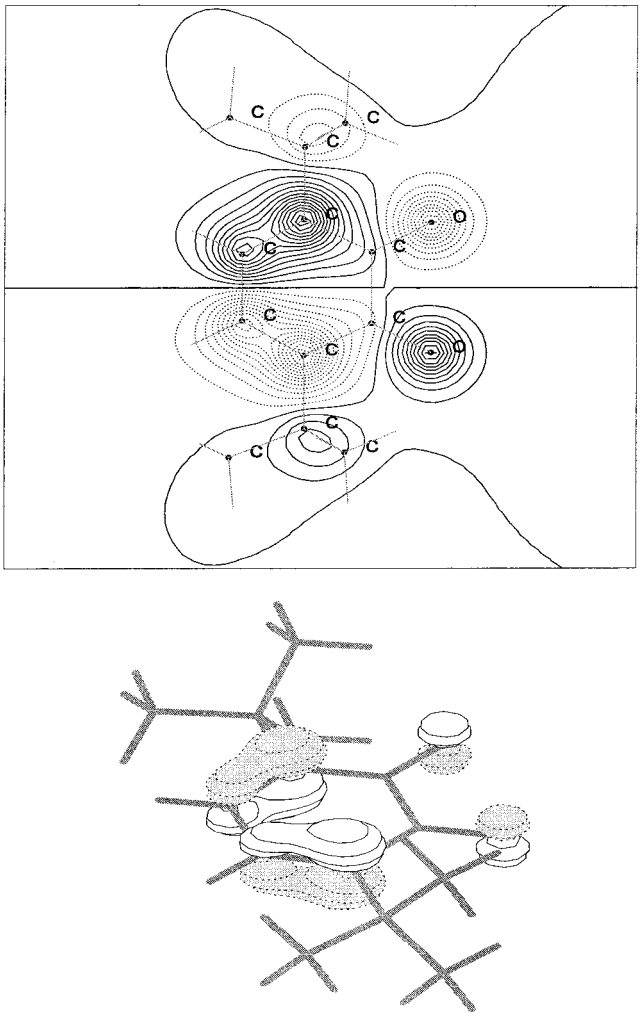

Figure 3. Semiquinone MO 58α. Top: Isovalue contour plot displaying the electron density obtained at the U-BLYP/6-311G** level. The contour is a slice taken 0.5 Å above the plane of the ring and shows the π-antibonding interaction between O(p_z) and C(p_z) orbitals. Bottom: MO 58α. The orbital density is mainly localized above and below the plane of the ring.

It is of particular interest to elucidate the spatial distribution of the HOMO (MO 61α) which hosts the only unpaired electron in semiquinone. This MO has main contributions from oxygen p_z orbitals and smaller contributions from C(p_z) orbitals of the six-membered ring. As shown in Figure 6, the electron density of MO 61α is localized above and below the plane of the ring. The contour shows the π-antibonding interaction between O(p_z) and C(p_z) orbitals and the π-bonding interaction within the C2−C3 and C1−C6 pairs. Due to its composition the HOMO can interact in a π fashion with metal orbitals of d_{xz} symmetry. The orbital composition of the semiquinone HOMO is similar to that of catechol. However, free catechol has one more electron than free semiquinone and, consequently, an equal number of α and β electrons. MOs 61α and 61β of catecholate have essentially equal composition and energy.[65] The occupancy of both of these MOs explains the diamagnetic character of the catecholate ligand. Furthermore, the single and double occupancy of semiquinone and catechol HOMOs, respectively, gives rise to the drastically different magnetic properties of [Cr(tren)(3,6-DTBSQ)]$^{2+}$ and [Cr(tren)(3,6-DTBCat)]$^{+}$ (vide infra).

(65) Wheeler, D. E.; Rodriguez, J. H.; McCusker, J. K. Manuscript in preparation.

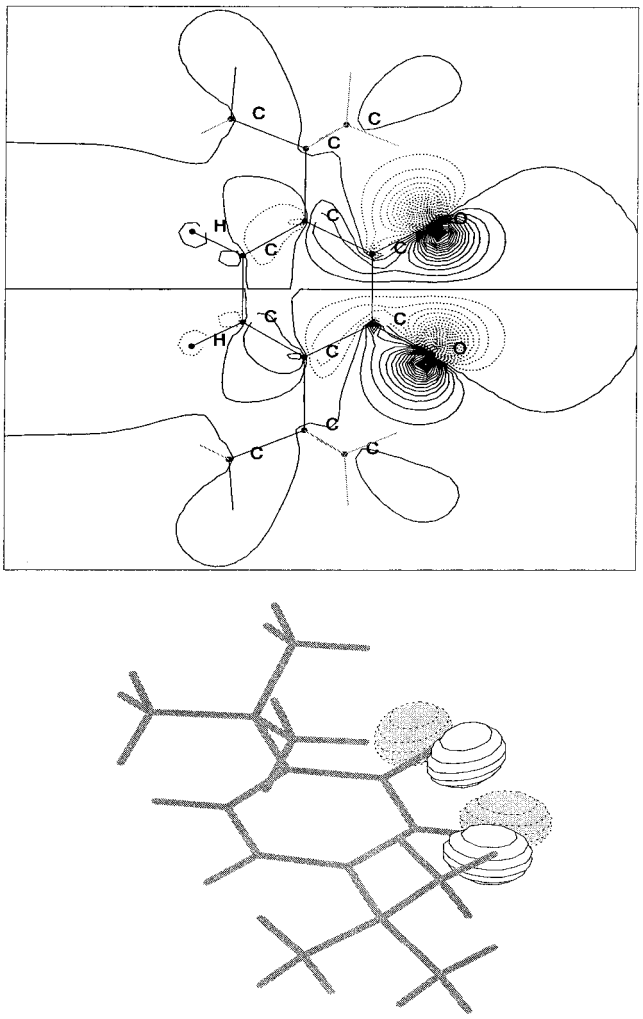

Figure 4. Semiquinone MO 59α. Top: Contour plot representing the electron density in the plane of the ring obtained at the U-BLYP/6-311G** level. The contour shows a weak σ-antibonding interaction between the oxygen orbitals. Bottom: MO 59α. The orbital lies in the *xy* plane with dominant p_y character.

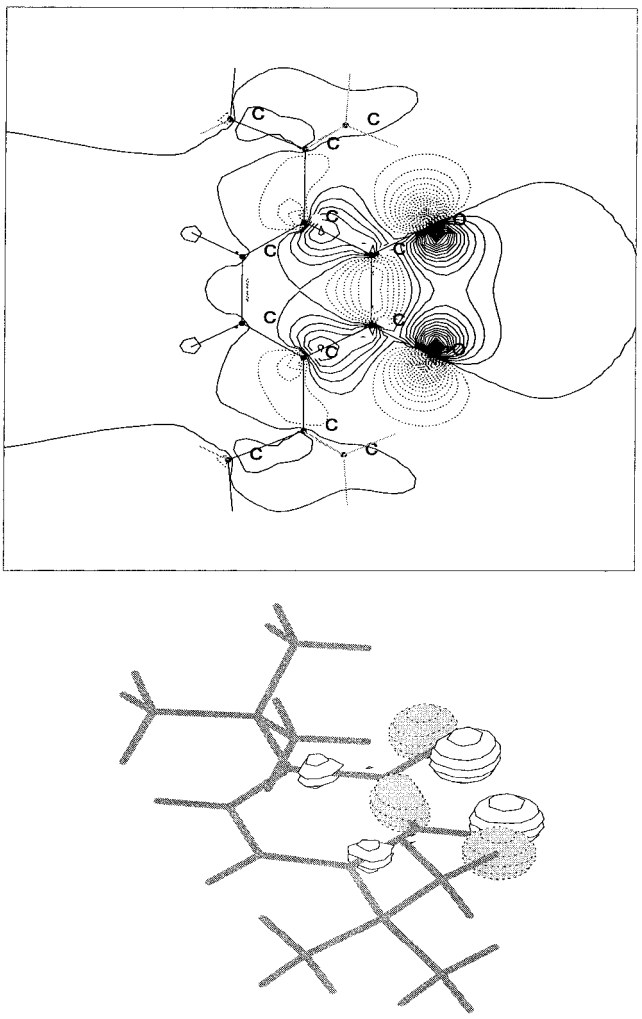

Figure 5. Semiquinone MO 60α. Top: Isovalue contour plot representing the electron density obtained at the U-BLYP/6-311G** level. The contour is a slice taken in the plane of the ring and shows the side-on antisymmetric combination of $O(p_y)$ and $C(p_y)$ orbitals. Bottom: MO 60α. The orbital density is mainly localized on the plane of the ring.

Virtual MO 62α is mostly composed of p_z orbitals from ring carbons C3 and C6. There are also smaller contributions from C1, C2, O1, and O2. This MO also has its electron density localized above and below the plane of the ring. The corresponding contour plot is shown in Figure 7. In contrast to the mixture of bonding and antibonding interactions encountered within the HOMO, MO 62α displays only π-antibonding interactions within the O−C, C2−C3, and C1−C6 pairs. The small $O(p_z)$ contributions to MO 62α allow a (weak) π interaction with metal orbitals of d_{xz} symmetry. We notice that virtual MO 62α is substantially higher in energy (i.e., 3.158 eV, Table 4) than occupied MO 61α.

The charge and spin densities of some semiquinone atoms, where the frontier MOs are mainly localized, are presented in Table 5. Most of the negative charge is localized on the oxygens whereas C1 and C2 have significant positive charge. This is consistent with the greater electronegativity of oxygen with respect to carbon. Since O1 and O2 are each bonded to one carbon and C1 and C2 are each bonded to two carbons and one oxygen, we expect negative charge concentration on the former and negative charge depletion on the latter. The rest of the ring carbons have lower negative charge. The spin density distribution of the semiquinone roughly reflects the composition of its HOMO. Accordingly, most of the spin density is localized on the oxygens. The rest of the spin is nearly equally distributed throughout the carbons of the six-membered ring. The NPA charges show greater polarization than the corresponding Mulliken charges. By contrast, the spin densities of both partitioning methods are closer to each other.

D. Electronic Structure of $[Cr(tren)(3,6\text{-}DTBSQ)]^{2+}$. (i) SCF Energies and Spin Expectation Values. The all electron 6-311G** basis set produced triplet (quintet) total energies of −2198.37578 (−2198.36346) and −2198.88873 (−2198.88178) hartrees for U-BLYP and U-B3LYP, respectively. Thus, the two different combinations of exchange-correlation functionals yielded a lower triplet total energy with respect to that of the quintet. These results are consistent with a triplet ground state, in agreement with magnetic susceptibility data (Section I). Although, as expected, we found some difference between the absolute energies calculated by the two exchange-correlation methods, we can compare their relative triplet−quintet splittings. We found that the three-parameter exchange of Becke plus Lee−Yang−Parr functionals (B3LYP) produced a lower triplet−quintet energy difference than BLYP.

The triplet state wave functions displayed some spin contamination due to admixture with the higher quintet. This effect was more noticeable for the U-B3LYP ($\langle S^2 \rangle = 2.90$) than for

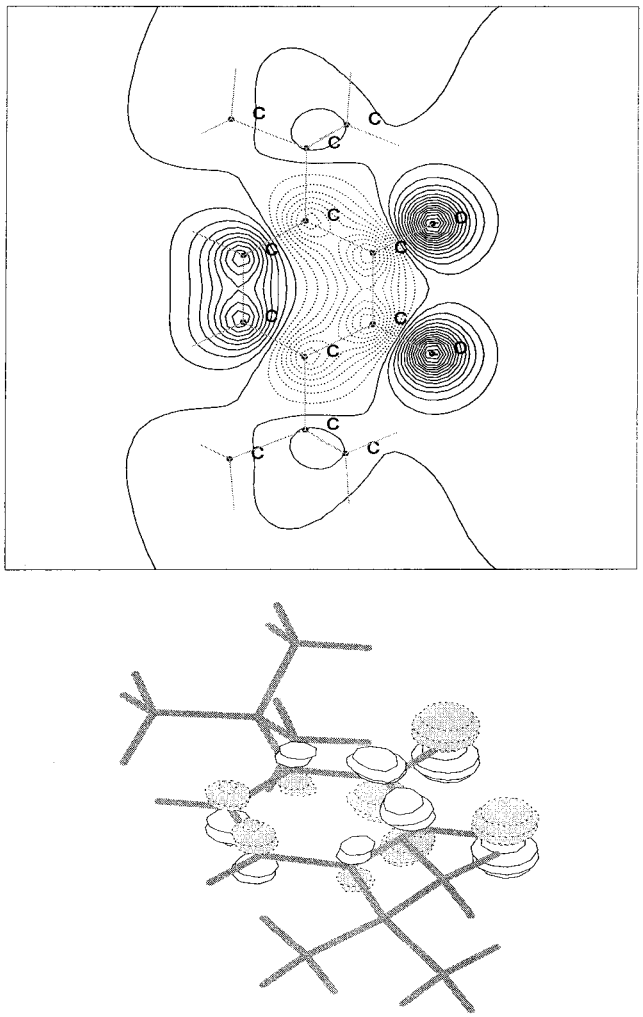

Figure 6. Semiquinone MO 61α (HOMO). Top: Isovalue contour plot representing the electron density obtained at the U-BLYP/6-311G** level. The contour is a slice taken at a plane 0.5 Å above the plane of the ring and shows the π-antibonding interaction between O(p_z) and C(p_z) orbitals. Bottom: HOMO. The orbital is localized above and below the plane of the ring.

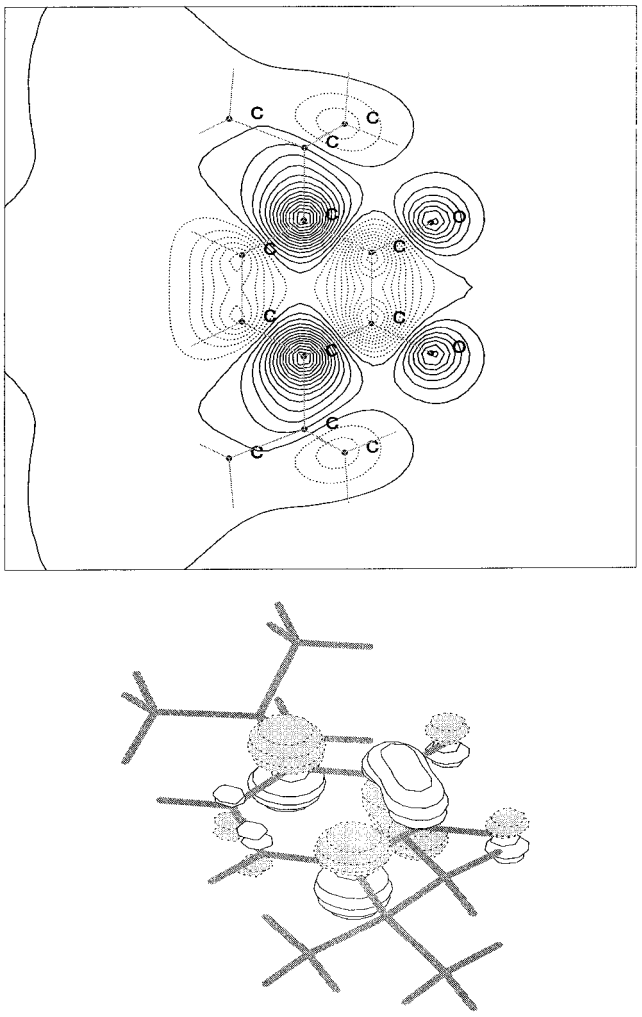

Figure 7. Semiquinone MO 62α. Top: Isovalue contour plot representing the electron density obtained at the U-BLYP/6-311G** level. The contour is a slice taken at a plane 0.5 Å above the plane of the ring and shows the π-antibonding interaction between O(p_z) and C(p_z) orbitals. Bottom: MO 62α. The orbital is localized above and below the plane of the ring.

the U-BLYP ($\langle S^2\rangle = 2.66$) SCF calculations. The expectation values of the total spin operator after spin annihilation[38,39] ($\langle S^2\rangle_A$) were very close to the value expected for a pure triplet state, indicating that only the quintet is significantly admixed with the triplet state. For the U-B3LYP and U-BLYP triplet wave functions the expectation values after spin annihilation were $\langle S^2\rangle_A = 2.02$ and 2.04, respectively. In agreement with what has been found for organic diradicals[36,37] and bimetallic complexes,[34] the ferromagnetic (i.e. quintet) wave functions represent a nearly pure spin state. In fact, the SCF quintet wave functions obtained at the U-B3LYP and U-BLYP levels displayed negligible spin contamination and yielded expectation values $\langle S^2\rangle \approx 6$.

(ii) Energies and Composition of Molecular Orbitals. Figure 8 and Table 6 show the energies and main composition of some frontier molecular orbitals corresponding to the U-BLYP/Φ_3^{UKS} wave function. The exchange interactions between the majority α electrons produce the stabilization of their MOs with respect to the corresponding β MOs which are higher in energy. MOs 113α and 114α are the HOMO and LUMO, respectively. The HOMO-LUMO energy gap obtained from the two exchange-correlation functionals was appreciably different, namely 0.801 and 2.174 eV for U-BLYP and U-B3LYP, respectively. Such a difference is expected due to the tendency of pure DFT methods to underestimate the HOMO-LUMO gap with respect to B3LYP, which includes Hartree−Fock exchange.

Table 5. Atomic Charge and Spin Densities of the Free Semiquinone Ligand Obtained at the U-BLYP/6-311G** Level

	NPA		Mulliken	
atom	charge	spin	charge	spin
O1	−0.632	+0.234	−0.373	+0.228
O2	−0.632	+0.234	−0.373	+0.228
C1	+0.355	+0.081	+0.141	+0.081
C2	+0.355	+0.081	+0.141	+0.081
C3	−0.118	+0.087	−0.059	+0.096
C4	−0.238	+0.096	−0.088	+0.105
C5	−0.238	+0.096	−0.088	+0.105
C6	−0.118	+0.087	−0.059	+0.096

The unrestricted SCF calculations for the triplet state included 113 α and 111 β occupied MOs. Therefore, MOs 112α and 113α are occupied whereas the corresponding β orbitals are unoccupied. The higher occupied and lower virtual molecular orbitals are mainly of metal or semiquinone character with little or negligible contribution from the tren ligand. The reference coordinate system used to describe the molecular orbitals is

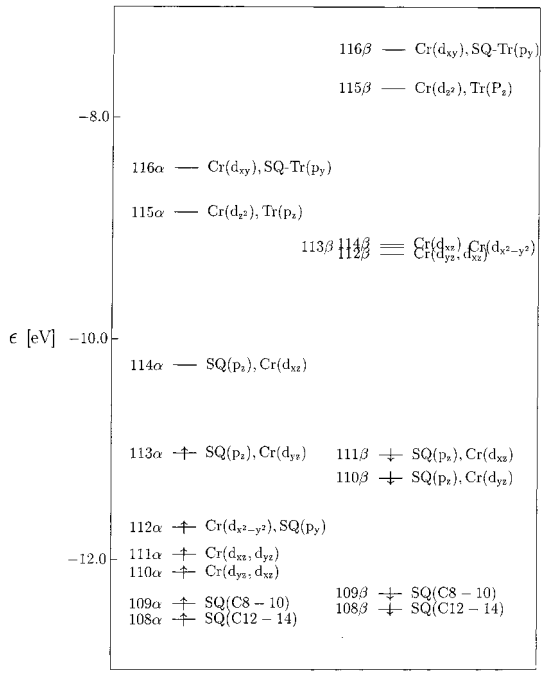

Figure 8. Energy level diagram for some frontier occupied and virtual molecular orbitals obtained at the U-BLYP/6-311G** level. The diagram shows the energies of some α and β orbitals from the triplet (antiferromagnetic) state wave function. The first atom (orbital) listed for MOs 110−116 has the main contribution to a molecular orbital. Tr represents the tren ligand. (C8−10) and (C12−14) indicate that MOs 108 and 109 are mainly distributed throughout carbons C8 to C10 and C12 to C14, respectively, but no information about their relative contributions is given for these atoms.

shown in Figure 2. In what follows we describe the composition of the frontier orbitals corresponding to the triplet state and U-BLYP since this method introduced less spin contamination than U-B3LYP.

MO 111α is mainly localized on the chromium ion (50.2%, Table 6) and has mainly d_{xz} symmetry. Consequently, the electron density corresponding to this orbital is above and below the O−Cr−O plane. This metal-centered MO only weakly interacts with semiquinone orbitals of p_z symmetry. MO 111β is the highest occupied from the β set of orbitals. As shown in Figure 9 and Table 6, this orbital is mostly localized on the semiquinone ligand with an additional contribution from Cr-(d_{xz}). The contour of Figure 9 is a slice taken 0.5 Å above the O−Cr−O plane and displays the π-bonding interaction between Cr(d_{xz}) and O(p_z) orbitals. The oxygen orbitals in turn overlap in a π-antibonding fashion with semiquinone (C1,C2)(p_z) orbitals. An inspection of the free ligand orbitals reveals that MO 111β is a symmetric combination of the semiquinone HOMO (Figure 6) and Cr(d_{xz}).

As shown in Figure 10 and Table 6, MO 112α is centered on the chromium ion (42.4%) and has $d_{x^2-y^2}$ symmetry. This orbital is characterized by an antisymmetric combination of metal and oxygen valence orbitals. The isovalue contour plot corresponding to MO 112α is a slice taken in the O−Cr−O plane and shows a distorted π-antibonding interaction between Cr($d_{x^2-y^2}$) and O(p_y) orbitals. The O1(p_y) orbital in turn combines with C1(p_y) in an antisymmetric fashion as do O2-(p_y) with C2(p_y). Inspection of the free semiquinone orbitals (Figure 5) reveals that MO 112α mainly originates from the combination of Cr($d_{x^2-y^2}$) and SQ(MO 60α).

MO 113α is the HOMO. Figure 11 and Table 6 reveal that this orbital is mostly localized on carbons C3 and C6 of the

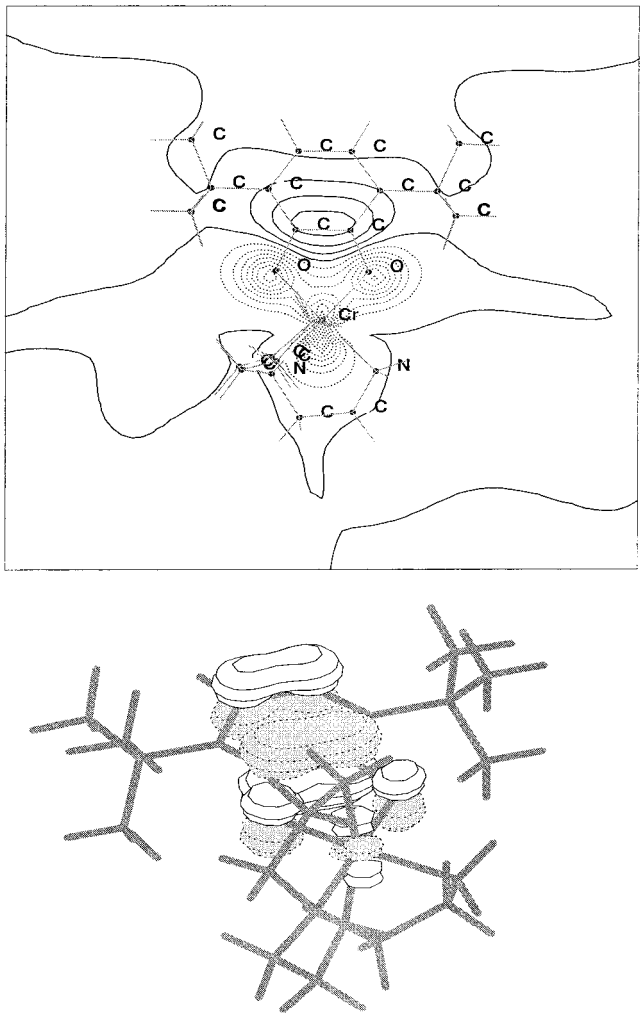

Figure 9. MO 111β of the Cr−semiquinone complex. Top: Isovalue contour plot obtained at the U-BLYP/6-311G** level. The plot shows the π-bonding interaction between chromium $3d_{xz}$ and oxygen p_z orbitals. The plane of the plot is 0.5 Å above the O−Cr−O plane. Bottom: Three-dimensional representation.

semiquinone ring with some admixture of Cr(d_{yz}). The contour plot is a slice parallel to the *z* axis and also to the line joining chromium and O1. It is displaced by 0.4 Å from the line joining chromium and O1 to show the weak π-antibonding interaction between Cr(d_{yz}) and O1(p_z) orbitals. The electron density of the HOMO is localized above and below the O−Cr−O plane since it is composed of metal and semiquinone orbitals which lie parallel to the *z* axis. An inspection of the free semiquinone orbitals (Figure 3) reveals that MO 113α corresponds to the antisymmetric combination of SQ(MO 58α) and Cr(d_{yz}).

The lowest unoccupied orbital (LUMO) is MO 114α. As shown in Figure 12 and Table 6, this orbital is mostly localized on the semiquinone ligand with main contributions from oxygen and carbon p_z orbitals. The contour of Figure 12 is taken 0.5 Å above the O−Cr−O plane and shows a π-antibonding interaction between O(p_z) and Cr(d_{xz}) orbitals. At the same time, there is a π-antibonding interaction between O(p_z) and orbitals C1(p_z) and C2(p_z). Accordingly, the electron density corresponding to MO 114α is localized above and below the O−Cr−O plane. An inspection of the free ligand orbitals reveals that MO 114α is an antisymmetric combination of the semiquinone HOMO (Figure 6) and Cr(d_{xz}).

Some interaction between chromium and the tren ligand can be found in MOs 115 and 116. Virtual MO 115α is localized

Table 6. Energies, Percent Contributions from Cr and Semiquinone Atoms O1, O2, C1, and C2, and Main Character of Frontier Molecular Orbitals Obtained from the U-BLYP/6-311G** Φ_3^{UKS} Wave Function for $[Cr(tren)(3,6\text{-}DTBSQ)]^{2+}$

orbital	type[a]	energy (eV)	% Cr	% O1	% O2	% C1	% C2	main character[b]
116α	V	−8.456	54.1	7.8	9.1	1.1	1.1	Cr(d_{xy}), SQ-Tr(p_y)
115α	V	−8.854	49.5	3.5	1.6	0.5	0.7	Cr(d_{z^2}), Tr(p_z)
114α	V	−10.238	6.9	12.8	15.2	10.7	10.2	SQ(p_z), Cr(d_{xz})
113α	O	−11.039	6.3	5.5	3.8	2.0	0.8	SQ(p_z), Cr(d_{yz})
112α	O	−11.707	42.4	8.2	7.3	2.5	2.1	Cr($d_{x^2-y^2}$), SQ(p_y)
111α	O	−11.958	50.2	0.1	1.1	0.1	5.1	Cr(d_{xz},d_{yz})
110α	O	−12.115	53.0	1.1	0.1	3.1	0.1	Cr(d_{yz},d_{xz})
109α	O	−12.400	4.0	0.7	3.0	1.2	1.3	SQ(C8−10)
108α	O	−12.543	12.6	2.2	0.1	1.5	1.5	SQ(C12−14), Cr($d_{x^2-y^2}$)
116β	V	−7.385	45.5	5.6	6.0	1.5	1.4	Cr(d_{xy}), SQ-Tr(p_y)
115β	V	−7.736	50.0	2.8	1.2	0.6	0.7	Cr(d_{z^2})
114β	V	−9.141	50.2	0.8	3.7	2.1	0.2	Cr(d_{xz},d_{yz})
113β	V	−9.173	52.9	2.4	1.9	2.6	2.7	Cr($d_{x^2-y^2}$)
112β	V	−9.234	48.3	2.6	0.6	0.1	1.6	Cr(d_{yz},d_{xz})
111β	O	−11.054	6.2	11.1	8.9	12.9	12.1	SQ(p_z), Cr(d_{xz})
110β	O	−11.264	1.3	2.9	3.6	2.9	4.2	SQ(p_z)
109β	O	−12.310	2.9	3.2	7.9	3.3	3.3	SQ(C8−10)
108β	O	−12.451	1.9	5.4	0.3	1.9	2.1	SQ(C12−14)

[a] V and O represent unoccupied (virtual) and occupied molecular orbitals, respectively. [b] The first atom (orbital) listed for MOs 110−116 has the main contribution to a molecular orbital. Tr represents the tren ligand. (C8−10) and (C12−14) indicate that MOs 108 and 109 are mainly distributed throughout carbons C8 to C10 and C12 to C14, respectively, but no percent information is given for these atoms.

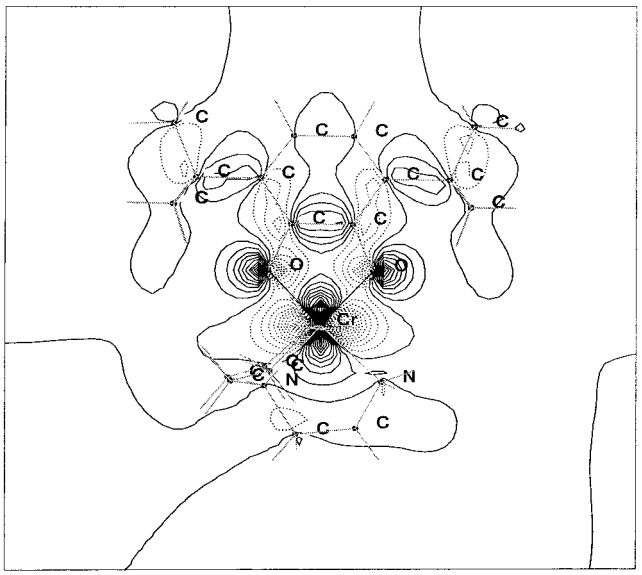

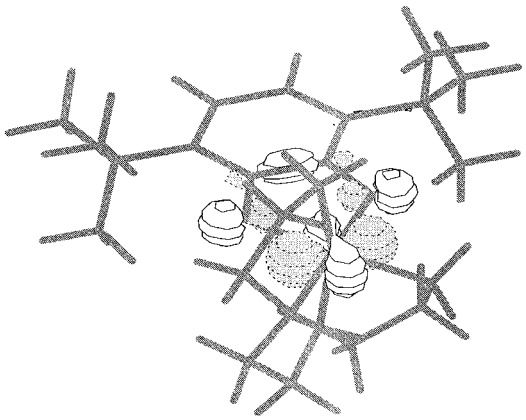

Figure 10. MO 112α of the Cr−semiquinone complex. Top: Isovalue contour obtained in the U-BLYP/6-311G** level. The plot represents the electron density at the O−Cr−O plane and displays the π-antibonding interaction between Cr($d_{x^2-y^2}$) and O(p_y) orbitals. Bottom: Three-dimensional representation.

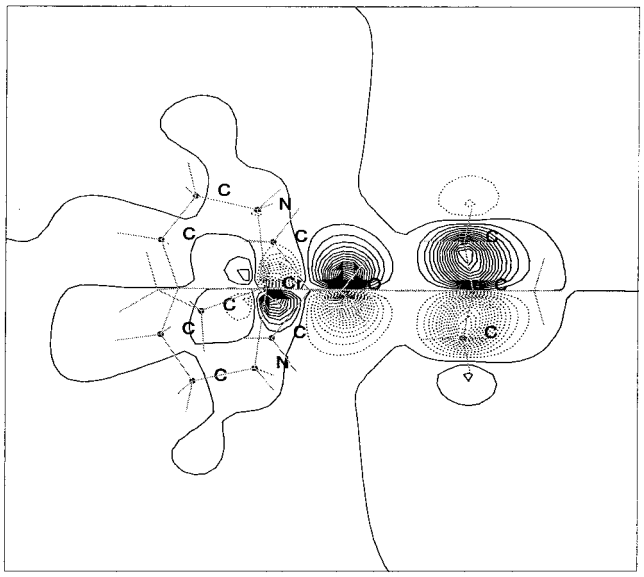

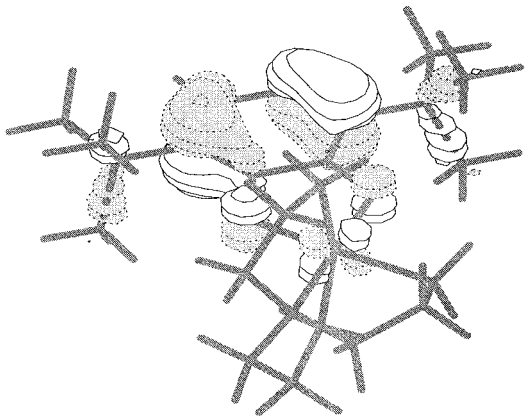

Figure 11. MO 113α of the Cr−semiquinone complex. Top: Isovalue contour plot obtained at the U-BLYP/6-311G** level. The plot corresponds to the HOMO. The plane is perpendicular to the O−Cr−O plane and is displaced 0.4 Å from the line joining chromium and O1. The figure displays the weak π-antibonding interaction between Cr-(d_{yz}) and O(p_z) orbitals. Bottom: Three-dimensional representation.

on the chromium ion (49.5%) and has d_{z^2} character (Figure 13, Table 6). This orbital also has contributions from p_z orbitals of the two nitrogens located above and below the O−Cr−O plane. The contour of Figure 13 is a slice of the electron density taken in the *yz* plane and shows the α-antibonding interaction

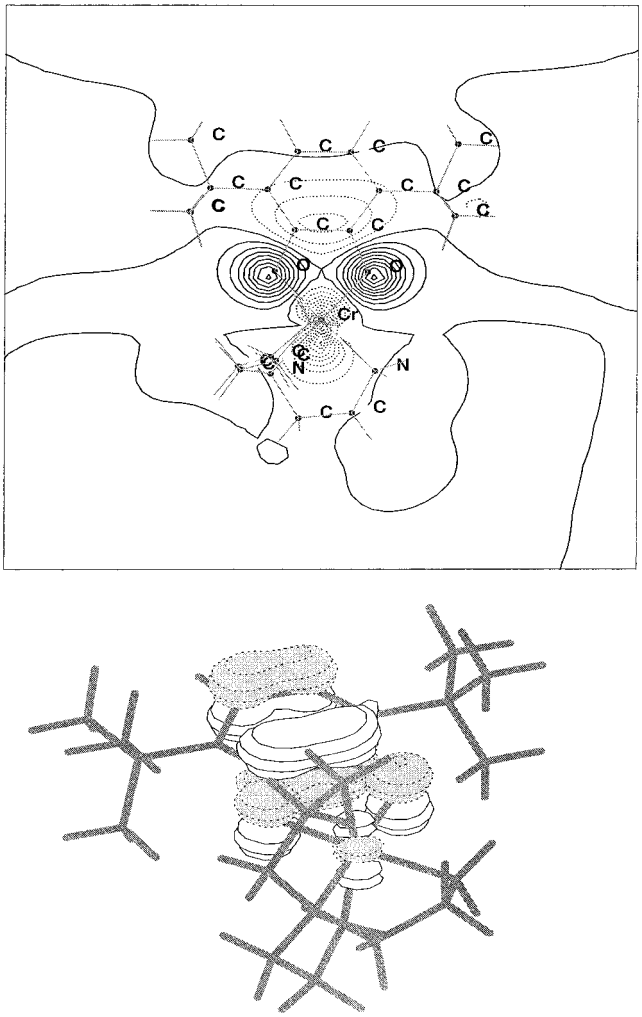

Figure 12. MO 114α of the Cr−semiquinone complex. Top: Isovalue contour plot obtained at the U-BLYP/6-311G** level. The plot corresponds to the LUMO. The plane is taken 0.5 Å above the O−Cr−O plane to display the π-antibonding interaction between Cr-(d_{xz}) and O(p_z) orbitals. Bottom: Three-dimensional representation.

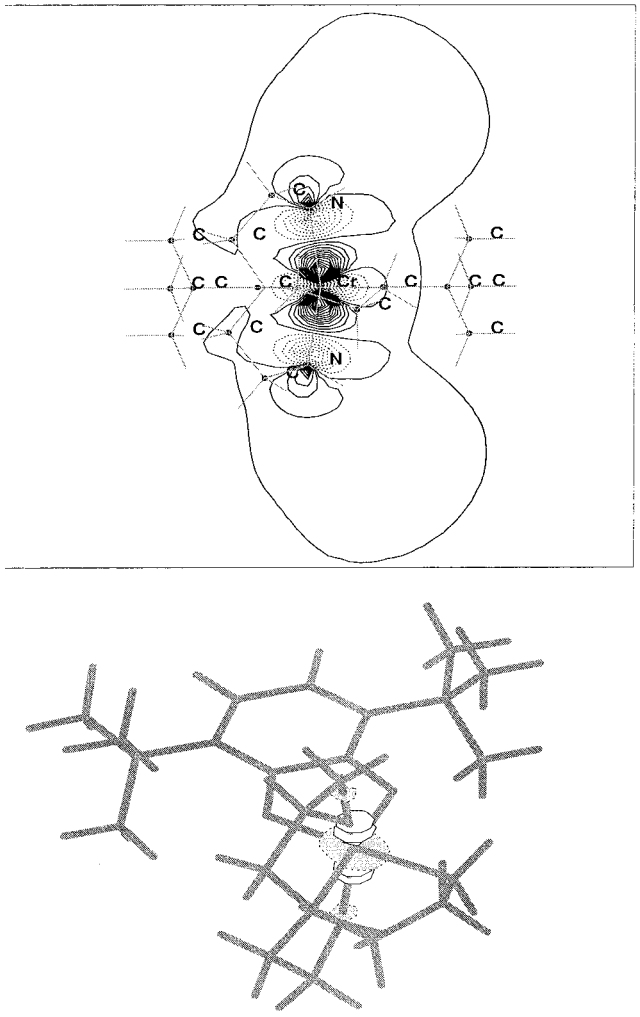

Figure 13. MO 115α of the Cr−semiquinone complex. Top: Isovalue contour plot obtained at the U-BLYP/6-311G** level. The plane of the plot is taken in the *yz* plane. The plot shows the σ-antibonding interaction between Cr(d_{z^2}) and N(p_z) orbitals from the tren ligand. Bottom: Three-dimensional representation.

between Cr(d_{z^2}) and (N2,N3)(p_z) orbitals. The d_{z^2} orbital, being perpendicular to the O−Cr−O plane, cannot interact strongly with O(p) orbitals and is essentially isolated from the semiquinone.

Virtual MO 116α is centered on the chromium ion (Figure 14) and has main d_{xy} character. There are also contributions from oxygen and nitrogen p orbitals. The contour of Figure 14 is a slice taken at the O−Cr−O plane that shows the σ-antibonding interaction between Cr(d_{xy}) and O(p) orbitals. A similar interaction is seen between Cr(d_{xy}) and (N1,N4)(p) orbitals. The metal d_{xy} orbital, therefore, interacts strongly not only with the semiquinone oxygens but also with the nitrogens on the tren. The strong σ-antibonding interaction of the metal with the four ligands in the *xy* plane produces the destabilization of MO 116α which is highest in energy among the metal-centered MOs. Inspection of the free ligand orbitals (Figure 4) reveals that MO 116α includes an antisymmetric combination of SQ(MO 59α) and Cr(d_{xy}).

(iii) Atomic Charge Densities. The NPA and Mulliken atomic charge densities are shown in Table 7. There was close agreement between the charges derived from the U-BLYP and U-B3LYP (not shown) wave functions. The latter method produced a slightly greater charge polarization; however, both exchange-correlation functionals yielded similar trends. In what follows we only discuss the analysis of the U-BLYP/6-311G** wave functions. As mentioned in Section II, the high spin (i.e., quintet) state can be described by a single determinant. The charge densities derived from the quintet wave function are free from possible effects of spin contamination and will be discussed first.

The NPA analysis of Φ_5^{UKS} assigned most of the positive charge to the chromium ion (+1.490). By contrast, all six atoms coordinated to the cation have negative charges in the −0.563 to −0.850 range. In particular, O1 and O2 have charges of −0.693 and −0.664, respectively. Within the semiquinone ring, some additional positive charge is localized on C1 and C2 (Table 7) whereas the rest of the ring carbons have smaller negative charge.

The NPA analysis of Φ_5^{UKS} indicates that the charge polarizations of the O−C bonds are slightly greater in the complex (Table 7) than in the free ligand (Table 5). This can be seen from the absolute values of the charges corresponding to O1, O2, C1, and C2. There is a greater relative change in the NPA charges corresponding to complexed C3, C4, C5, and C6 which are approximately half of those of the free ligand. The Mulliken analysis produced a greater difference between the polarizations of the O−C bond in free and complexed semiquinone. For the free ligand, C1 and C2 each have a Mulliken charge of +0.141

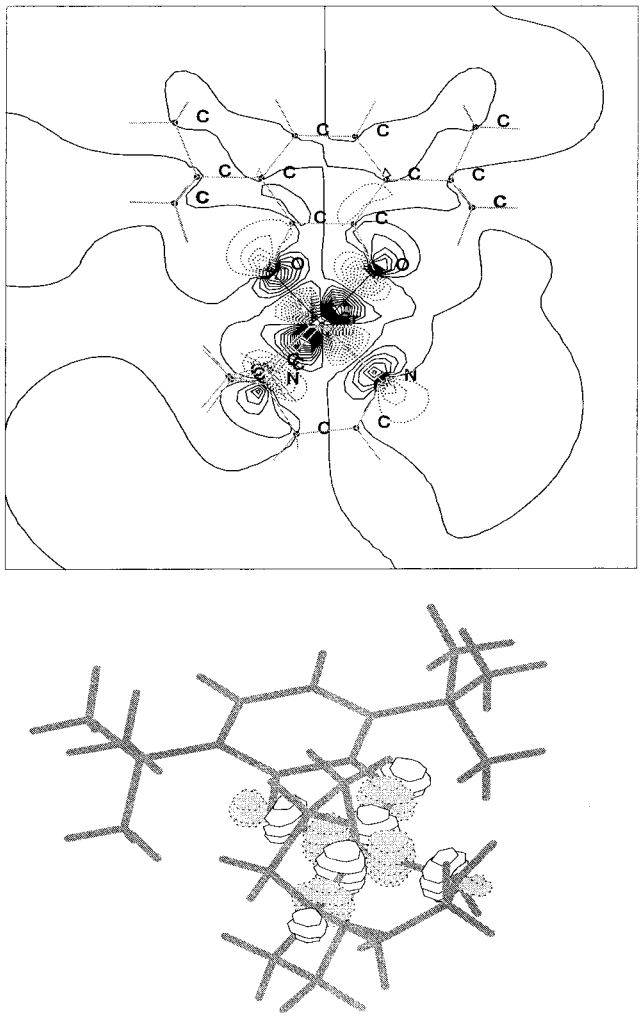

Figure 14. MO 116α of the Cr−semiquinone complex. Top: Isovalue contour plot obtained at the U-BLYP/6-311G** level. The plot is a slice taken in the O−Cr−O plane and shows the σ-antibonding interaction between Cr(d_{xy}) and p orbitals from the semiquinone oxygens and from two nitrogens of the tren ligand. Bottom: Three-dimensional representation.

whereas O1 and O2 each have a charge of −0.373. Upon complexation, C1 and C2 have Mulliken charges of +0.188 and +0.241, respectively, whereas O1 and O2 have charges of −0.545 and −0.523. Therefore, an important trend is reproduced by both methods of charge partitioning, namely that upon complexation C1 and C2 become more positive whereas O1 and O2 become more negative. Although NPA and Mulliken charges display many similar trends, there are also some subtle differences. For example, the NPA charges are more polarized within the semiquinone ring than the corresponding Mulliken charges. It is also significant that the NPA charges clearly distinguish N1 (−0.563) from the other three, nearly equivalent, more negative nitrogens coordinated to the metal. In contrast, the Mulliken analysis assigned very similar charges to all four nitrogens. Figure 1 shows N1 coordinated to three carbons whereas the rest of the nitrogens are each coordinated to two carbons and two hydrogens (not shown). Considering that the electronegativity difference between nitrogens and hydrogens is greater than that between nitrogens and carbons, it is reasonable to expect that N1 will be less negative than the other three nitrogens, in agreement with the NPA analysis.

As shown in Table 7, the NPA charges derived from triplet and quintet wave functions are close to each other in magnitude and have equal signs. The quintet charges are, in general, slightly more polarized. The same trends previously described for the quintet state are also found for the triplet state. This indicates that no substantial rearrangement of atomic charge accompanies a triplet to quintet transition since MOs 111β, occupied in the triplet state, and 114α, occupied in the quintet, have very similar composition.

(iv) Atomic Spin Densities. Table 7 shows the NPA and Mulliken spin densities localized on the chromium center, nitrogen ligands, and some of the semiquinone atoms. The positive and negative signs, which are the signs of the net spin density $\rho_S = \rho(\alpha) - \rho(\beta)$, represent a net α or β character, respectively. Similar trends were found for the U-BLYP and U-B3LYP (not shown) densities. The latter method yielded a slightly greater spin polarization. In what follows, we discuss the results derived from the Φ_5^{UKS} and Φ_3^{UKS} wave functions obtained at the U-BLYP/6-311G** level.

The spin populations obtained from Φ_5^{UKS} are particularly important since this wave function is free from admixture of other spin states. The total (NPA) α spin at the chromium ion is +2.986, fully consistent with a quartet spin configuration. With the exception of C3 and C6, which have an almost negligible β density, all other semiquinone atoms listed in Table 7 have substantial α character. C1 and C2 are the atoms with greater spin (+0.216 and +0.222, respectively) with somewhat lower α densities nearly equally assigned to O1, O2, C4, and C5. The net NPA spin density of the semiquinone atoms listed in Table 7 (oxygens plus ring carbons) is +1.068. By contrast, the four nitrogen ligands are nearly diamagnetic with a combined total spin of −0.104. Overall, all atoms of the tren have negligible spin densities.

The total molecular spin derived from the Φ_5^{UKS} wave function is +4 units. This is a necessary result of our calculations which imposed convergence to a quintet state. However, the fact that about three units of spin are localized on the chromium and one unit of spin is localized on the semiquinone confirms that the complex under study can be described as a system where the Cr($S = {}^3/_2$) ion is spin coupled to the SQ($S = {}^1/_2$) ligand. The spin densities derived from the Φ_5^{UKS} wave function correspond to the ferromagnetic (high spin) state where the chromium ion and semiquinone have net parallel spins.

We can compare the spin distributions of the semiquinone ligand before (Table 5) and after (Table 7) complexation. The total NPA spin of the atoms listed in Table 5 (oxygens plus ring carbons) for the free ligand is 0.996 units, slightly lower than the corresponding spin of +1.068 determined previously for the complexed ligand. Thus, no significant amount of semiquinone spin is gained upon complexation. The spin density of the free ligand is mostly localized on the oxygen atoms, consistent with the main O(p_z) character of the semiquinone HOMO that hosts its only unpaired electron. The NPA analysis assigned a total of +0.468 units of spin to both oxygens before and +0.347 units after complexation. C1 and C2 were assigned a total of +0.162 units before and +0.438 units after complexation. Thus, there is an important difference between the spin distributions of free and complexed semiquinones, namely that the atoms with greater spin density in the free ligand are O1 and O2 whereas the atoms with greater spin in the complexed ligand are C1 and C2. We also notice that the free ligand has atoms C3, C4, C5, and C6 with nearly equal spin densities. Upon complexation, C4 and C5 acquire and enhanced α character whereas C3 and C6 have a weak β character. Even though the net spin densities of C3 and C6 are small, all

Table 7. Atomic Charge and Spin Densities Obtained from U-BLYP/6-311G** Wave Functions of [Cr(tren)(3,6-DTBSQ)]$^{2+}$

	Φ_3^{UKS}				Φ_5^{UKS}			
	NPA		Mulliken		NPA		Mulliken	
atom	charge	spin	charge	spin	charge	spin	charge	spin
Cr1	+1.462	+2.808	+1.415	+2.798	+1.490	+2.986	+1.425	+2.975
O1	−0.674	−0.116	−0.536	−0.117	−0.693	+0.166	−0.545	+0.152
O2	−0.631	−0.135	−0.506	−0.136	−0.664	+0.181	−0.523	+0.165
C1	+0.350	−0.162	+0.185	−0.176	+0.360	+0.216	+0.188	+0.239
C2	+0.361	−0.162	+0.230	−0.174	+0.380	+0.222	+0.241	+0.244
C3	−0.054	+0.018	−0.012	+0.036	−0.064	−0.016	−0.016	−0.036
C4	−0.132	−0.092	−0.037	−0.101	−0.115	+0.150	−0.029	+0.164
C5	−0.112	−0.133	−0.040	−0.149	−0.104	+0.180	−0.036	+0.199
C6	−0.072	+0.038	−0.002	+0.059	−0.075	−0.030	−0.003	−0.054
N1	−0.560	−0.029	−0.578	−0.034	−0.563	−0.032	−0.578	−0.036
N2	−0.842	−0.026	−0.591	−0.032	−0.846	−0.023	−0.592	−0.028
N3	−0.838	−0.027	−0.589	−0.033	−0.842	−0.023	−0.591	−0.029
N4	−0.849	−0.024	−0.586	−0.028	−0.850	−0.026	−0.586	−0.031

population analyses of ligated semiquinone consistently assigned a spin of opposite sign to these two atoms with respect to the other ring carbons.

The spin densities derived from the Φ_3^{UKS} wave function are also shown in Table 7. The absolute values corresponding to the triplet state are close to those found for the quintet which, in general, are slightly larger. However, the signs of the spin densities of the semiquinone atoms change with respect to those of the quintet to yield the triplet configuration. The effects of the quintet contaminant on the spin populations derived from the U-BLYP Φ_3^{UKS} wave function are not expected to be large.[66] Nevertheless, since the contamination introduces some uncertainty, we mostly focus on the qualitative aspects of the population analyses. The NPA analysis assigned almost all of the α spin (+2.808) to the chromium ion, which is close to the +3 units expected for a quartet spin configuration. Most of the β density is distributed between carbons C1, C2, C4, and C5 of the semiquinone ring. A lesser amount of β spin is localized on the oxygens. The total spin assigned to the oxygens and ring carbons is −0.744 units. The nitrogen ligands show very small β densities and, therefore, are not significant sources of molecular magnetism. The total molecular spin is +2 units. Again, this is a necessary result of the calculations that required convergence to a triplet state. However, the net α and β spin assigned to the chromium ion and semiquinone are close to what is expected for their quartet and doublet states, respectively. At the same time, there is no major spin density associated with the tren. Therefore, the spin densities derived from the triplet wave functions are consistent with an antiferromagnetic (low spin)[67] configuration where the Cr($S = {}^3/_2$) ion and SQ($S = {}^1/_2$) radical are spin coupled and have net antiparallel spins. Table 7 shows how the spin polarization of the main semiquinone atoms is reversed in sign (from β to α) in going from the triplet to the quintet. The same is not true for the nitrogen ligands that display very weak β character for both triplet and quintet states. We also notice that, in general, Table 7 shows close agreement between the spin densities determined from NPA and Mulliken population analyses.

(v) Natural Atomic Orbital Occupancies. Table 8 displays the total occupancy and net spin of the valence natural atomic orbitals (NAOs) for the atoms involved in spin coupling. The α and β occupations can be found from the total occupancy and net spin columns of Table 8. Although the occupancies of the atomic orbitals have non-integer values in the molecular environment, we can relate the effective atomic configurations to idealized atomic states with idealized electron configurations.[57,58,68]

We first discuss the NPA analysis of Φ_5^{UKS}. The occupation of the three lower energy valence NAOs of chromium is close to unity, consistent with an idealized $d^1_{yz}d^1_{xz}d^1_{x^2-y^2}$ configuration of the ion. However, the occupation of the higher energy NAOs is significantly higher ($d^{0.699}_{xy}d^{0.565}_{z^2}$) than the idealized $d^0_{xy}d^0_{z^2}$ configuration. This can arise from the distorted octahedral environment,[69] which mixes the ligand field orbitals, and from covalency. The chromium NAOs have predominantly α character. While the three lowest energy orbitals are mostly populated by α electrons, the two higher energy d orbitals have a greater relative β occupation and, consequently, a low net α spin. The occupancies of d_{xy} and d_{z^2} reflect some electron delocalization from the ligands toward the cation. Although the occupancy of the 4s orbital is low in comparison to the d orbitals, it is nevertheless significant. NAO 4s has an almost negligible α spin, indicating an almost equal occupation of α and β electrons.

The occupancies of the 2s and 2p oxygen NAOs are close in value, within a 1.520 to 1.773 range, with $2p_x$ having the lowest population. Most of the oxygen NAOs have nearly equal α and β occupancies reflecting the nearly diamagnetic character of these orbitals. However, the analysis of Φ_5^{UKS} yields a net α spin associated with the $2p_z$ orbitals of both oxygens. The occupancies of the NAOs of C1 and C2 are close to or below unity, in sharp contrast with the corresponding oxygen populations which are closer to two electrons. The $2p_z$ orbitals of C1

(66) The effect of the quintet admixture on the charge and spin populations derived from our triplet U-BLYP Kohn−Sham wave function is not expected to be significant.[72] The validity and application of some spin projection methods[38,39] developed for some conventional ab-initio wave functions (e.g., MP2) to assess the effects of spin contamination on population analyses of Kohn−Sham wave functions is at present doubtful[41,73,74] and possibly unnecessary.[72] In our opinion, such methods overcorrect the relative spin density distributions of the complex under study. Note also that U-BLYP does not include Hartree−Fock exchange (included in U-B3LYP) and is therefore free from spin contamination effects intrinsic to UHF.

(67) Our use of the term *antiferromagnetic* for the triplet state refers to the overall spin configuration of the complex that has *net* α and β spin densities localized on the chromium ion and semiquinone ligand, respectively. Low spin states of magnetic solids with net magnetization are referred to by solid state authors as *ferrimagnetic* and can be considered a particular case of antiferromagnetism. See, for example, Harrison[75] for definitions used in solid state theory. In the magnetism of biological and inorganic trasition metal clusters it is common to refer to low spin states of spin coupled systems as antiferromagnetic even though these are not necessarily diamagnetic. See, for example, Kahn (p 120).[31]

(68) Weinhold, F. *NBO 4.0 Program Manual*; Theoretical Chemistry Institute, University of Wisconsin: Madison, 1996.

(69) Rodriguez, J. H.; Ok, H. N.; Xia, Y. M.; Debrunner, P. G.; Hinrichs, B. E.; Meyer, T.; Packard, *N. J. Phys. Chem.* **1996**, *100*, 6849.

Table 8. Natural Atomic Orbital (NAO) Analysis[57−59] of U-BLYP/6-311G** Wave Functions of $[Cr(tren)(3,6\text{-DTBSQ})]^{2+}$ and $[Cr(tren)(3,6\text{-DTBCat})]^{+}$

		$[Cr(tren)(3,6\text{-DTBSQ})]^{2+}$				$[Cr(tren)(3,6\text{-DTBCat})]^{+}$	
		Φ_3^{UKS}		Φ_5^{UKS}		Φ_4^{UKS}	
atom	NAO	occup	spin	occup	spin	occup	spin
Cr	4s	0.252	+0.013	0.253	+0.012	0.255	+0.011
	$3d_{z^2}$	0.572	+0.099	0.565	+0.098	0.580	+0.130
	$3d_{xy}$	0.703	+0.307	0.699	+0.305	0.745	+0.345
	$3d_{x^2-y^2}$	0.918	+0.691	0.918	+0.687	0.894	+0.655
	$3d_{yz}$	1.039	+0.935	1.039	+0.933	1.050	+0.876
	$3d_{xz}$	1.045	+0.763	1.028	+0.948	1.144	+0.770
O1	2s	1.712	−0.000	1.713	+0.004	1.716	+0.005
	$2p_x$	1.524	−0.003	1.520	−0.005	1.539	−0.021
	$2p_y$	1.774	−0.009	1.773	−0.006	1.713	+0.002
	$2p_z$	1.657	−0.103	1.680	+0.171	1.759	+0.089
O2	2s	1.707	+0.000	1.706	+0.005	1.712	+0.004
	$2p_x$	1.550	−0.016	1.544	−0.014	1.514	−0.002
	$2p_y$	1.750	+0.002	1.745	+0.003	1.734	−0.019
	$2p_z$	1.615	−0.121	1.660	+0.185	1.773	+0.084
C1	2s	0.844	−0.005	0.846	+0.006	0.811	0.000
	$2p_x$	0.784	+0.002	0.787	+0.002	0.936	0.000
	$2p_y$	1.062	+0.002	1.061	+0.001	0.938	+0.004
	$2p_z$	0.935	−0.161	0.920	+0.206	1.034	+0.011
C2	2s	0.843	−0.005	0.846	+0.007	0.808	0.000
	$2p_x$	0.906	−0.001	0.908	+0.001	0.787	+0.003
	$2p_y$	0.939	+0.006	0.940	+0.003	1.094	+0.001
	$2p_z$	0.925	−0.163	0.901	+0.211	1.038	+0.013
C3	2s	0.883	+0.002	0.883	−0.002	0.866	0.000
	$2p_x$	1.058	+0.003	1.059	−0.006	1.070	−0.001
	$2p_y$	1.108	+0.001	1.110	−0.001	1.071	0.000
	$2p_z$	0.984	+0.013	0.990	−0.006	1.027	+0.012
C4	2s	0.952	−0.003	0.954	+0.005	0.893	0.000
	$2p_x$	1.182	−0.002	1.182	+0.002	1.122	0.000
	$2p_y$	1.059	+0.001	1.058	−0.001	1.128	0.000
	$2p_z$	0.925	−0.088	0.907	+0.143	1.028	+0.015
C5	2s	0.954	−0.005	0.955	+0.006	0.889	0.000
	$2p_x$	1.132	−0.003	1.133	+0.003	1.171	0.000
	$2p_y$	1.105	0.000	1.104	0.000	1.087	0.000
	$2p_z$	0.907	−0.124	0.899	+0.170	1.027	+0.014
C6	2s	0.881	+0.003	0.882	−0.003	0.864	0.000
	$2p_x$	1.075	+0.003	1.075	−0.006	1.069	−0.001
	$2p_y$	1.095	+0.002	1.096	−0.003	1.084	0.000
	$2p_z$	1.000	+0.030	1.001	−0.019	1.025	+0.013

and C2 are the individual orbitals with greater α spin in the semiquinone. The rest of C1 and C2 NAOs have negligible spin. The occupancy of the NAOs for the rest of the ring carbons is also close to unity. C4 and C5 have $2p_z$ orbitals with appreciable α character whereas the rest of their orbitals have negligible spin. It is interesting that all NAOs of C3 and C6 display a very weak β character, opposite to the rest of the carbons of the six-membered ring which, in general, have NAOs with net α character.

As shown in Table 8, the NPA analysis of Φ_3^{UKS} indicates that the total occupancies of the NAOs in the triplet state are close to those of the quintet. This is true for the chromium ion and also for the semiquinone atoms. However, there are obvious and significant differences between the relative occupations by α and β electrons of some NAOs. In general, the chromium NAOs in the triplet state have a net α spin very close in magnitude to that of the corresponding quintet NAOs. However, we notice that for the triplet state $3d_{xz}$ has a net spin of +0.763, which corresponds to α and β occupancies of 0.904 and 0.141, respectively. For the quintet this orbital has a net spin of +0.948, corresponding to α and β occupancies of 0.988 and 0.040, respectively. This is consistent with the composition of MOs 111α and 111β. In the triplet state, these two MOs are occupied, 111β essentially being the free semiquinone HOMO with some additional $3d_{xz}$ character. In the quintet state MO 111β is no longer occupied. Therefore, the greater β occupation of NAO $3d_{xz}$ in the triplet state, with respect to the quintet, reflects the fact that some finite amount of β electron density is delocalized from the semiquinone HOMO toward the cation. Similarly, the almost negligible β occupancy of NAO $3d_{xz}$ in the quintet state reflects the fact that even though MO 111β has some $3d_{xz}$ character, it is no longer occupied. Therefore, in the quintet state there is no β density to be transferred from the semiquinone HOMO to the cation. Table 8 clearly shows that in the triplet state the semiquinone NAOs with greater β spin are of p_z symmetry. By contrast, the NAOs of C3 and C6 have very weak character.

(vi) Exchange Coupling of $[Cr(tren)(3,6\text{-DTBSQ})]^{2+}$. In what follows we relate some of the previous results to the molecular spin configurations of the triplet and quintet states.

The NPA and Mulliken atomic populations are consistent with a triplet state that has two distinct spatial localizations for the net α and β spin densities. We found that the α density is localized on the chromium center which has close to +3 units of spin, corresponding to a Cr($S = {}^3/_2$) configuration. The β density is mainly concentrated at two of the carbons of the semiquinone ring (i.e., C1 and C2) and to a lesser extent at O1, O2, C4, and C5. The total β density of the ring carbons and oxygen atoms approaches the −1 units of spin that correspond to the SQ($S = {}^1/_2$) configuration. The tren ligand is essentially diamagnetic. The atomic spin density distribution of the triplet state is, therefore, fully consistent with a net antiferromagnetic spin coupling between the chromium ion and the semiquinone radical.[67] Some β density from the semiquinone oxygens appears to be lost by delocalization toward the cation. The NPA analysis in terms of NAOs provides further insight about the specific orbitals involved in spin coupling and the effects of β delocalization. We found that in the triplet state NAO $3d_{xz}$, which has mostly α occupation, also has some β occupancy. This suggests that the net antiferromagnetic spin configuration of the chromium−semiquinone complex arises, at least in part, from partial β delocalization from the semiquinone toward an α occupied $3d_{xz}$ orbital. Indeed, the occupancy and composition of MOs 111α and 111β is consistent with this picture. As seen in Table 6, occupied MO 111α is centered on the chromium ion with mainly $3d_{xz}$ character. Occupied MO 111β is mainly composed of the semiquinone HOMO with some additional $3d_{xz}$ contribution. This latter MO can be described as a π-bonding interaction between the semiquinone HOMO and Cr($3d_{xz}$). The bonding character of MO 111β allows some β density to be shared between the ligand and the cation as is graphically shown in Figure 9. Thus, the overlap of the semiquinone HOMO, which hosts a β electron, with Cr($3d_{xz}$), which hosts an α electron, allows partial β delocalization toward the cation, giving rise to an antiparallel alignment of their electron spins and to a net triplet state.

We found that the NPA and Mulliken atomic spin densities corresponding to the quintet state also assigned nearly +3 units of spin to the chromium ion. The total spin assigned to the ring carbons of the semiquinone plus oxygens was close to +1 units. Thus, the α spin is clearly localized on two distinct regions of the complex. Furthermore, the net spin of the semiquinone reverses in sign in going from the triplet to the quintet whereas the tren ligand remains very nearly diamagnetic. The spin density distribution of the quintet state is, therefore, fully consistent with a net ferromagnetic spin coupling between

Table 9. Difference between the Triplet and Quintet Self-Consistent-Field Energies and Calculated Heisenberg Exchange Constant J for $[Cr(tren)(3,6\text{-DTBSQ})]^{2+}$

	U-BLYP (cm^{-1})	U-B3LYP (cm^{-1})
$\lvert E_5^{UKS} - E_3^{UKS}\rvert^a$	+2704	+1528
$\lvert E_5^{PUKS} - E_3^{PUKS}\rvert^b$	+3235	+1971
J^c	+1618	+986

[a] Calculated from values of total SCF energies given in the text (Section IVD). [b] Calculated from values of total SCF energies given in the text (Section IVD) after the approximate spin projection of eq 11. [c] Calculated from eq 6 and ($\lvert E_5^{PUKS} - E_3^{PUKS}\rvert$).

the chromium ion and the semiquinone. The NPA analysis for the quintet indicates that NAO $3d_{xz}$ has α and β occupancies very close to 1 and 0, respectively. This is related to the lack of β delocalization from the semiquinone HOMO since MO 111β is unoccupied. Instead, in the quintet state MO 114α becomes occupied. This latter MO is mainly localized on the ligand and corresponds to a π-antibonding interaction between the semiquinone HOMO and Cr($3d_{xz}$). The antibonding nature of MO 114α precludes extensive electron density to be localized in the region between the cation and the semiquinone as is graphically shown in Figure 12. The previous observations indicate that the slightly lower absolute values of the spin densities found for the triplet state with respect to the quintet are related to the delocalization of some β density from the semiquinone toward the cation. This delocalization will reduce the net β spin of the semiquinone as well as the net α spin of the cation.

The total SCF energies reported above were used to determine the triplet−quintet energy separation $\lvert E_5^{UKS} - E_3^{UKS}\rvert$. An application of eq 11 produced the projected triplet energy and, using $E_5^{UKS} \approx E_5^{PUKS}$, the value of $\lvert E_5^{PUKS} - E_3^{PUKS}\rvert$ was also determined (Table 9). As previously discussed, the quintet wave function represents an essentially pure spin state. The triplet−quintet energy gaps obtained from the U-BLYP and U-B3LYP methods were closer to each other after the triplet energy corrections than before such correction was applied (Table 9). This observation reflects the greater amount of spin contamination encountered for the U-B3LYP than for the U-BLYP triplet wave functions. The quantity $\lvert E_5^{PUKS} - E_3^{PUKS}\rvert$ was in turn used to calculate the magnitude of the exchange constant J from eq 6. The values obtained for J which correspond to the U-BLYP and U-B3LYP energies were +1618 and +986 cm^{-1}, respectively (Table 9). To assess the effects of spin contamination, J was also calculated from the unprojected energy $\lvert E_5^{UKS} - E_3^{UKS}\rvert$. We found that the unprojected values of J were ≈20% (i.e., 1351.9 cm^{-1}) and ≈23% (i.e., 763.8 cm^{-1}) lower than the projected values for U-BLYP and U-B3LYP, respectively.

The values for J given in Table 9 compare well with the lower limit estimated for $[Cr(tren)(3,6\text{-DTBSQ})](PF_6)_2$ by Wheeler *et al.*[7] and for $[Cr(CTH)(DTBSQ)]_2Cl(PF_6)_3$ by Benelli *et al.*[5] (i.e., $>+700$ cm^{-1}) based on their experimental data. In addition, the calculations of Benelli *et al.*[5] based on the Tanabe formalism yielded the value $J \approx 800$ cm^{-1}. This result is well within our projected and unprojected U-B3LYP values for J, which can be taken as higher and lower limits, respectively. Adams *et al.*[6] have recently calculated the exchange coupling for the high spin $Co^{II}(SQ)_2(phen)$ complex. These authors determined[6] a value for J of +1188 cm^{-1} for the coupling between the cobalt ion and each of the two semiquinone ligands. Therefore, these two first-row transition metals (i.e., Cr and Co) are strongly antiferromagnetically coupled to their semiquinone ligands.

To gain some insight about the relationship between geometry and magnitude of exchange coupling, we performed additional U-B3LYP/LanL2DZ SCF calculations varying the Cr−O and O−C bond lengths by ±0.10 and ±0.07 Å, respectively. The bond lengths were chosen so that the bonding angles remain constant. Therefore, any variations in the magnitude of J are related to the varying bond lengths and not to the symmetry of the orbitals, which remains unchanged. As the bond distances increased, the magnitude of J decreased by ≈37%. Inversely, as the bond lengths were decreased by the same amount, the magnitude of J increased by ≈63%. Thus, the magnitude of J increases faster with decreasing distances than it decreases with increasing distances. Although our limited data did not allow us to find a quantitative relation for J as a function of distance, it appears to be consistent with the nearly exponentially decaying behavior that has been noticed for a variety of spin coupled organic[37] and metallic[70,71] compounds.

E. Electronic Structure of $[Cr(tren)(3,6\text{-DTBCat})]^+$. (i) Composition of Molecular Orbitals. The free catechol ligand has one more electron than the free semiquinone. MOs 61α and 61β (not shown) are the catechol HOMOs and have virtually identical composition and energy.[65] At the same time, these two orbitals are very similar in composition to the semiquinone HOMO shown in Figure 6.

The determinantal wave function corresponding to the quartet state of the catecholate complex includes 114α and 111β occupied molecular orbitals. Overall, the frontier MOs (not shown) of the catecholate complex are similar in composition to the orbitals of the semiquinone complex (Table 6). For example, MO 114α is mainly localized on the ligand and corresponds to a π-antibonding interaction between a catecholate HOMO and Cr(d_{xz}). Therefore, this occupied MO has essentially the same composition as the unoccupied MO 114α of the semiquinone complex (Figure 12). However, in the catecholate complex MO 114α also includes a minor admixture of Cr(d_{xy}) character. MO 111β is mainly localized on the catechol and represents the π-bonding interaction between a catecholate HOMO and Cr(d_{xz}). Therefore, occupied MO 111β is similar in composition to the corresponding orbital of the semiquinone complex (Figure 9). However, in the catecholate complex MO 111β also includes a minor admixture of Cr(d_{yz}) character. The overall diamagnetic character of ligated catechol arises from the occupation of MOs 114α and 111β which being of nearly equal composition have a combined net spin close to zero.

(ii) Atomic Charge and Spin Densities. Table 10 shows the atomic charge densities derived from the quartet state wave function. The NPA analysis assigned most of the positive charge to the chromium ion. Both oxygens have substantial and nearly equal negative charge. C1 and C2 have some additional positive charge whereas the rest of the ring carbons all have low negative charge. While the NPA analysis roughly assigned three times more negative charge to C4 and C5 than to C3 and C6, the corresponding Mulliken charges are very close to each other. Since C4 and C5 are each bonded to two carbons and C3 and C6 are each bonded to three carbons, we expect the former pair to be more negatively charged than the latter in agreement with the NPA analysis. Similarly, the NPA charges of all four nitrogen ligands are of the same order of magnitude

(70) Gorun, S. M.; Lippard, S. J. *Inorg. Chem.* **1991**, *30*, 1625.
(71) Wang, C.; Fink, K.; Staemmler, V. *Chem. Phys.* **1995**, *201*, 87.
(72) O. Ventura, Personal communication, 1998.
(73) D. Fox, Personal communication, 1997.
(74) B. Schlegel, Personal communication, 1998.
(75) Harrison, W. A. *Solid State Theory*; Dover: New York, 1979.

Table 10. Atomic Charge and Spin Densities of $[Cr(tren)(3,6\text{-DTBCat})]^+$ Obtained at the U-BLYP/6-311G** Level

	NPA		Mulliken	
atom	charge	spin	charge	spin
Cr	+1.323	+2.788	+1.316	+2.777
O1	−0.734	+0.075	−0.592	+0.065
O2	−0.740	+0.067	−0.591	+0.057
C1	+0.258	+0.016	+0.189	+0.021
C2	+0.250	+0.017	+0.161	+0.022
C3	−0.054	+0.011	−0.043	+0.013
C4	−0.184	+0.015	−0.061	+0.016
C5	−0.188	+0.015	−0.053	+0.015
C6	−0.061	+0.012	−0.059	+0.013
N1	−0.523	−0.019	−0.576	−0.021
N2	−0.780	−0.012	−0.569	−0.018
N3	−0.767	−0.016	−0.561	−0.021
N4	−0.807	−0.015	−0.581	−0.015

but the charge assigned to N1 is lower as expected from electronegativity arguments. By contrast, the Mulliken charges do not distinguish N1 from the other nitrogens.

The additional unit of charge of the catechol ligand does not greatly affect the absolute values of the individual atomic charge densities of the complex. The total NPA charge of chromium (+1.323) is not much lower than its charge in the semiquinone complex (≈+1.462). The total charge of both oxygens in ligated catecholate (−1.474) is not significantly greater than their total charge (≈−1.305) in ligated semiquinone. Some greater negative charge is assigned to C4 and C5 of ligated catechol than the corresponding charges of ligated semiquinone whereas the positive charge of C1 and C2 is somewhat lower for the former oxidation state. Therefore, the extra charge associated with the reduction from ligated semiquinone to ligated catecholate is distributed throughout the ligand, roughly reflecting the composition of a catecholate HOMO. There should also be some charge delocalization toward the cation as was previously discussed for the semiquinone complex. This delocalization tends to lower the net positive charge of chromium as well as the net negative charge of the ligand. In fact, the previous observations also reflect the higher degree of covalency of the chromium−catecholate bond. The difference between charges assigned to the cation in catechol and semiquinone complexes is consistent with the shorter Cr−O bonds (determined from X-ray diffraction) in the former (average 1.911 Å) and the longer bonds of the latter (average 1.928 Å). Shorter Cr−O bond lengths permit greater electron delocalization toward the cation, thereby lowering its net positive charge.

The atomic spin distributions (Table 10) for the quartet wave function are fully consistent with an idealized Cr($S = {}^3/_2$)−catechol($S = 0$) formulation of the complex. The NPA spin density at the chromium ion (+2.788) approaches the value of +3 units of spin corresponding to a quartet state. At the same time, both NPA and Mulliken population analyses clearly show that the spin density throughout the six-membered ring of ligated catechol is negligible. This is in sharp contrast to the net spin densities assigned to C1, C2, C4, and C5 of ligated semiquinone (Table 7). There is some minor α spin associated with each of the two oxygens (≈+0.07) that is about half the spin density of each oxygen in the semiquinone complex.

(iii) Natural Atomic Orbital Occupancies. Cr($3d_{xz}$) and, to a lesser extent, Cr($3d_{xy}$) are the valence NAOs of chromium that display the greater difference in occupancy between catecholate and semiquinone complexes. These two NAOs have greater total occupancy in the former complex than in the latter (Table 8). The additional occupancy is of β character for Cr($3d_{xz}$) and of α character for Cr($3d_{xy}$). We have already established that the extra electron of the catecholate complex is mainly localized on a catecholate HOMO with greater and lesser admixtures of Cr($3d_{xz}$) and Cr($3d_{xy}$), respectively (i.e., MO 114α). Therefore, the extra α occupancy of NAO Cr($3d_{xy}$) is related, at least in part, to delocalization toward the cation via MO 114α. Similarly, the extra β occupancy of NAO Cr($3d_{xz}$) is related, at least in part, to delocalization from the ligand toward the cation via MO 111β as in the case of the semiquinone complex. The greater β occupancy of NAO Cr($3d_{xz}$) in the catechol complex, with respect to the semiquinone, can arise from its shorter Cr−O bond lengths that allow for greater covalency.

The extra electron of the catecholate complex is delocalized throughout the ligand according to the composition of MO 114α. The effect of this electron on the occupancy of the NAOs is subtle but noticeable. The $2p_z$ orbitals of O1, O2, C1, C2, C4, and C5 each have about 0.1 greater occupancy than in the semiquinone complex. This effect is not very noticeable for C3 and C6 since their $2p_z$ orbitals do not contribute as much to the catecholate HOMOs.

V. Conclusions

We have performed computationally demanding non-local gradient-corrected self-consistent field DFT calculations on chromium−semiquinone and chromium−catechol complexes. The energies, molecular orbital compositions, atomic charges, and spin densities that have emerged from these calculations provide a detailed picture of the chromium−semiquinone and chromium−catecholate bonds. In what follows we summarize some of the findings and conclusions of this work:

(i) The spin densities derived for the chromium−semiquinone complex from triplet and quintet wave functions are consistent, qualitatively and quantitatively, with those expected for the antiferromagnetic and ferromagnetic states, respectively, of the Heisenberg model. The NPA and Mulliken analyses clearly show net α and β densities localized at the chromium ion and semiquinone, respectively. By contrast, the tren ligand is essentially diamagnetic.

(ii) The symmetric and antisymmetric combinations of the semiquinone HOMO and Cr(d_{xz}) produce π-bonding and π-antibonding molecular orbitals, respectively, which are mainly of semiquinone character and about 6.2% chromium. In the triplet state only the bonding orbital is occupied (i.e., MO 111β). The direct overlap between the semiquinone HOMO and Cr(d_{xz}) allows partial delocalization toward the cation and favors the antiparallel alignment of their electron spins. The spin density corresponding to the partially delocalized electron remains mainly on the ligand which has close to −1 units of spin.

(iii) We have determined theoretical values for the Heisenberg constant (J) that quantifies antiferromagnetic exchange between the chromium and semiquinone spin centers. The U-B3LYP formalism produced a lower value than U-BLYP. At the same time, the values obtained from the U-B3LYP calculations (i.e., ≈986 cm^{-1}) compare well with estimates made by previous authors (i.e., ≈800 cm^{-1})[5] based on experimental data.

(iv) The strength of J appears to follow a nearly exponential decay as the Cr−O and O−C bond lengths simultaneously increase.

(v) The spin density of the free semiquinone is mainly localized on the oxygen atoms. This reflects the composition of the semiquinone HOMO. Upon complexation, the absolute values of the spin densities at the oxygens decrease reflecting some β delocalization toward the cation.

(vi) The overall diamagnetic character of ligated catechol arises from the occupancy of MOs 114α and 111β which are mainly composed of the free catecholate HOMOs with some additional metal character. Having nearly equal composition, these MOs yield a combined spin density close to zero.

(vii) While a purely ionic picture assigns +3 units of charge to the chromium ion, the NPA and Mulliken charges of the covalent semiquinone and catechol complexes are substantially lower. This reflects the covalent nature of the metal−oxygen bonds which allow for significant charge delocalization. This effect is more noticeable for the catecholate complex due to its shorter Cr−O bond lengths.

(viii) In general, NPA and Mulliken population analyses show similar trends, the former displaying greater charge polarization. However, there are subtle but noticeable instances where the NPA analysis produces results more consistent with electronegativity arguments. One clear example is the NPA charge assigned to N1, a tertiary amine, which is lower than the charge assigned to the other nitrogens, all of which are primary amines. By comparison, the Mulliken charges fail to significantly distinguish the charge of N1.

Acknowledgment. We thank the helpful comments made by Prof. P. G. Debrunner. The authors gratefully acknowledge the National Science Foundation (CHE-9729003) and the Alfred P. Sloan Foundation (J.K.M.) for financial support. The computational work was made possible by computer allocation grants from the Research Computing Cluster (RCC) of the University of Illinois, the National Center for Supercomputer Applications (NCSA), and Mahui High Performance Computing Center (MHPCC).

Supporting Information Available: Tables of positional parameters, anisotropic displacement factors, bond distances, and bond angles; table with optimized Cartesian coordinates of $[Cr(tren)(3,6\text{-}DTBSQ)]^{2+}$ at the U-B3LYP/LanL2DZ level (20 pages, print/PDF). See any current masthead page for ordering instructions and Web access information.

JA980917M